

Copyright
by
Jonas Traphöner
2014

**The Thesis Committee for Jonas Traphöner
Certifies that this is the approved version of the following thesis:**

**Evaluation of Impedance Parameters
in Transmission Lines**

**APPROVED BY
SUPERVISING COMMITTEE:**

Supervisor:

Surya Santoso

Mircea Driga

**Evaluation of Impedance Parameters
in Transmission Lines**

by

Jonas Traphöner, B.E.

Thesis

Presented to the Faculty of the Graduate School of

The University of Texas at Austin

in Partial Fulfillment

of the Requirements

for the Degree of

Master of Science in Engineering

The University of Texas at Austin

August 2014

Dedication

This work is dedicated to my family who supports me no matter where in the world I may be. Their love, trust, guidance, and support made me strive to pursue the goals that I set for myself. My father's meticulous work style and my mother's faith and confidence inspire me to this day, and always will. I also dedicate this work to my Opa Wörmann, who is a passionate traveller, hobby broker and historian. He taught me to go out into the world, get out of my comfort zone and to never stop learning.

Acknowledgements

Above all, my thanks and sincere gratitude belong to my advisor, Dr. Surya Santoso who has given me the opportunity to strengthen and deepen my knowledge in the field of energy systems by letting me work in his research group and allowing me to be a Teaching Assistant. I am grateful for the in depth knowledge and guidance that Dr. Santoso has provided me with throughout my studies. Working under him has been an incredible learning experience and his feedback and encouragement has made me excel immensely in my academic endeavors.

I would also like to thank Dr. Mircea Driga for his guidance and support throughout my graduate studies. Finally, I want to thank all of my lab members who have given me good laughs, productive and interesting discussions about culture, engineering and energy systems, and who have become my friends throughout our studies. Thank you Swagata Das, Min Lwin, Anamika Dubey, Pisitpol Chirapongsananurak, David Orn Jonsson, Kyung Woo Min, Yichuan Niu and Tuan Ngo.

Abstract

Evaluation of Impedance Parameters in Transmission Lines

Jonas Traphöner, M.S.E.

The University of Texas at Austin, 2014

Supervisor: Surya Santoso

A more accurate and flexible grid analysis is achieved through an adaptive and dynamic calculation of line parameters. This is needed for future smart grid implementation. The primary objective of this thesis is to analyze the calculation of transmission line parameters. The impact certain assumptions have on the accuracy of line parameters and fault location algorithms are evaluated. In particular, the impact of the grounded shield wire assumption on the accuracy of fault location algorithms is analyzed. This implies that the impedance of towers be taken into consideration, rather than the simplification of a direct connection of the earth wire to ground. Secondly, the phenomenon of skin-effect is analyzed and evaluated in regards to a more accurate representation of line parameters and a minimization of parameter inaccuracy. Accuracy of line parameters, particularly zero- sequence line impedance is subject to many uncertainties. This stems from the fact that zero-sequence line impedance depends on

earth resistivity along with tower grounding impedances, which tend to be estimated in common calculation techniques. A simple test case, which consists of a 3.73 mile long transmission line with two shield wires and a tower footing resistance every 0.19 miles, was set up to evaluate the assumption of grounding shield wire. The analysis shows that tower footing resistance affects only the zero-sequence line impedance. This leads to a marginal increase in error from one-ended impedance-based methods in locating single line-to-ground or double line-to-ground faults. On the other hand, fault location estimates from two-ended methods are not affected as they do not make use of the zero-sequence line impedance in fault location computation.

Skin effect does not have any significant impact on line parameters when standard transmission line frequencies of 0 to 60 Hz are analyzed. The change in internal reactance and resistance size is insignificant compared to larger frequencies. However, if the conductor radius is increased, skin-effect increases and thus might have a considerable impact on reactance and resistance values. Overall, this work identifies the necessity to re-evaluate and update line parameter calculations when increasing computational power is available.

Table of Contents

List of Tables	x
List of Figures	xi
1. INTRODUCTION	1
1.1. Motivation and Objective	1
1.2. Approach	2
1.3. Results	2
1.4. Contribution	4
2. THEORETICAL LINE PARAMETER CALCULATION	5
2.1. Direct- Current Resistance of Conductors	6
2.2. Inductance of a Transmission Line	7
2.2.1. Three- Phase Three Wire System	11
2.2.2. Conductor Stranding	12
2.2.3. Transposition	14
2.2.4. Bundling	15
2.3. Capacitance of a Transmission Line	16
2.3.1. Three- Phase Three Wire System	19
2.3.2. Conductor Stranding and Transposition	21
2.3.3. Bundling	21
2.4. Short, Medium and Long Lines	22
3. IMPACTS ON LINE PARAMETERS	26
3.1. Varying Earth Resistivity	26
3.2. Varying Transposition of the Line	28
3.3. Varying Length of the Transmission Line	29
3.4. Carson's Model	31
3.5. Kron Reduction	32
4. ASSUMPTIONS IN FAULT LOCATION ALGORITHMS	34
4.1. Fault Location Algorithms	34

4.2. Grounding of Shield Wire Assumption	35
4.2.1. Benchmark Test Case: 69-kV Single Circuit Transmission Line.....	36
4.2.2. Impact on the Accuracy of Fault Location Algorithms	40
5. FREQUENCY VARIATION IN THE TRANSMISSION LINE	45
5.1 Skin Effect	45
5.2 Impedance Variation Through Changes in Frequency	51
6. CONCLUSION	56
6.1. Summary of Data Analysis	56
6.2. Future Work	58
BIBLIOGRAPHY	59

List of Tables

Table 4. 1: Conductor Data	39
Table 4. 2: Impact of Tower Footing Resistance on the Eriksson Method.....	41
Table 4. 3: Estimates from the Two-ended Unsynchronized Two-ended Method	44

List of Figures

Figure 2. 1: Transmission line model	5
Figure 2. 2: Resistance of a cylindrical conductor	6
Figure 2. 3: Conductor with external magnetic field.....	8
Figure 2. 4: Cross-section of a conductor	9
Figure 2. 5: Stranded Conductors	12
Figure 2. 6: Subconductors of a Transmission Line	13
Figure 2. 7: Transposition of phase conductors.....	14
Figure 2. 8: Conductor Bundling.....	15
Figure 2. 9: Visualization of Gauss's law	16
Figure 2. 10: Electric Field of a charged conductor.....	17
Figure 2. 11: Short- Line Model.....	23
Figure 2. 12: Medium- Length Line Model.....	24
Figure 3. 1: Resistivity across various earth sections.....	27
Figure 3. 2: Transmission line on a hill.....	28
Figure 3. 3: Dip in Transmission Line	29
Figure 3. 4: Spiraling of a Conductor	30
Figure 3. 5: Earth- return conductors underneath ground	32
Figure 3. 6: 4- Wire Transmission System.....	33
Figure 4. 1: Fault- Locating Mechanism	35
Figure 4. 2: Shield Wire Grounded through a Finite Value of Tower Footing Resistance	36
Figure 4. 3: 69-kV Single circuit Transmission Line Test Case	37
Figure 4. 4: Overhead Line Spacing in Feet	38

Figure 4. 5: Transmission Line Modeled as an n-phase Model in PSCAD with Two Shield Wires Grounded through a Tower Footing Resistance R_T	39
Figure 4. 6: Estimates from Eriksson Method. Tower Footing Resistance = 0 Ω indicates that the tower is grounded directly	40
Figure 4. 7: Effect of Tower Footing Resistance on Sequence Line Impedances. Tower Footing Resistance Affects the Zero-sequence Line Impedance Only	42
Figure 4. 8: Impedance Scan Function Used in PSCAD to Calculate the Zero- sequence Impedance of the Transmission Line at Different Values of Tower Footing Resistance	43
Figure 4. 9: Tower Grounding Resistance Has no Impact on the Accuracy of Two-ended Eriksson Method	43
Figure 5. 1: Visualization of Skin Effect [18]	46
Figure 5. 2: Internal conductor current distribution for 20 Hz, 50 Hz, and 60 Hz	50
Figure 5. 3: Internal conductor current distribution for 400 Hz	50
Figure 5. 4: Reactance Dependency on Frequency for a 5mm conductor	52
Figure 5. 5: Resistance Dependency on Frequency for a 5mm conductor	52
Figure 5. 6: Reactance Dependency on Frequency up to 400 Hz	53
Figure 5. 7: Resistance Dependency on Frequency up to 400 Hz	53
Figure 5. 8: Reactance Dependency for various Conductor Sizes	54
Figure 5. 9: Resistance Dependency for various Conductor Sizes	55

1. INTRODUCTION

1.1. MOTIVATION AND OBJECTIVE

With the trend towards smarter and real-time electricity grid monitoring and technology, earlier approaches of transmission line parameter calculation need to be updated. Modern computing techniques render assumptions for manual computation of line parameters calculation obsolete. In particular, the re-evaluation of line parameter calculations paves the way to a more accurate analysis of the electricity grid. This is required when smart grid technology or protection devices such as Intelligent Electronic Devices (IEDs) are incorporated into the electricity power grid.

The primary objective of this thesis is to analyze the calculation of transmission line parameters and evaluate the impact certain assumptions have on the accuracy of line parameters and fault location algorithms. In particular, the impact of the grounded shield wire assumption on the accuracy of fault location algorithms in IEDs is considered. The evaluation takes the impedance of tower footing into consideration and neglects the simplification of a direct connection of the earth wire to ground. Secondly, the phenomenon of skin effect is analyzed and evaluated in regards to a more accurate representation of line parameters and a minimization of parameter inaccuracy. This work also analyzes the accuracy of line parameters, particularly zero- sequence line impedance, which is subject to many uncertainties. This stems from the fact that zero-sequence line impedance depends on earth resistivity along with tower grounding impedances, which tend to be estimated in common calculation techniques.

1.2. APPROACH

The work documented in this thesis is initially approached from a purely theoretical standpoint. The details of current line parameter calculations are covered to fully understand the development of various simplifications that exist in the procedure. Chapter 2 provides a detailed derivation of the various line parameters. Chapter 3 gives a general overview and insight into the assumptions and simplifications that are performed in transmission line parameter calculations. A basic introduction to various fault location algorithms is described in the beginning of Chapter 4, so that the ultimate target of improving fault location algorithms is fully understood. Following, the impact of grounded shield wire assumption is evaluated based on a developed PSCAD/EMTDC model and fault location algorithms in MATLAB. The generated model in PSCAD simulations with various tower groundings are run, the results implemented into available MATLAB code, and the accuracies of fault location analyzed. Finally, in Chapter 6 the phenomenon of skin effect and inaccuracies of estimated line parameters are analyzed and evaluated. For the purpose of improving fault location estimates, this detailed analysis of line parameter inaccuracies, and in particular the effect of grounding of shield wire assumption, is performed.

1.3. RESULTS

A 69-kV test feeder, an example circuit described in IEEE C37.114 Standard [1], was adopted to analyze the impact of tower footing resistance on the accuracy of fault location algorithms. The results for each of the various grounding of shield wire scenarios

are discussed and illustrated in detail in Chapter 5 and 6. Results show that the grounding of shield wire through a resistance has no impact on the accuracy of two-ended fault location algorithms. This stems from the fact that two-ended fault location algorithms do not use zero-sequence parameters. One-ended fault location algorithms are affected by tower grounding, but the error is insignificant. The error remains almost the same for various tower resistances. The size and the number of towers between the monitoring locations do not have a significant impact on the accuracy of one-ended methods. When analyzing the obtained results of skin effect, it can be seen that in general, the conductor's line parameter calculations are hardly affected for frequencies up to 60 Hz. However, if the conductor radius is increased significantly, the skin effect plays a greater role, even in lower frequency environments. Hence, if conductors consist of thick wires, the skin effect might lead to significant inaccuracies in the calculation of internal line parameters.

1.4. CONTRIBUTION

The dynamic calculation of line parameters provides a more accurate and flexible grid analysis, which is needed for future smart grid implementation. Since classical textbooks have not yet addressed the inaccuracies of fault location algorithms in regard to the grounding shield wire assumption, this analysis is novel. Improved modeling techniques are available (e.g. n phase), but they have not gained popularity due to their complexity compared with traditional methods. Skin effect is neglected in standardized line parameter calculations, but is taken into consideration in this thesis. This approach identifies the necessity to reevaluate and update line parameter calculations when increasing computational power is available.

2. THEORETICAL LINE PARAMETER CALCULATION

In order to plan, construct and operate a transmission line grid appropriately, it is necessary to anticipate the phenomena and losses that occur on the grid along with the simplifications and assumptions that can be made to calculate the essential line parameter values. Complex transmission lines with various conductors, multiple strands, bundling and varying tower height can be represented and taken into account through extensive calculations. The basic transmission line model consists of the five parameters: series resistance, series-inductance, mutual-inductance, shunt-capacitance and shunt-conductance [2]. The values of these parameters can be calculated by analyzing the physical properties of the transmission line wire, tower configuration, and environment in which the grid is operating. Basic principles of electric- and magnetic- field theory are applied. In the following chapter a detailed description and calculation of these parameters is introduced. This extensive derivation is necessary to fully comprehend the line parameter simplifications that are performed throughout the parameter calculation, while also serving as a review of commonly known techniques.

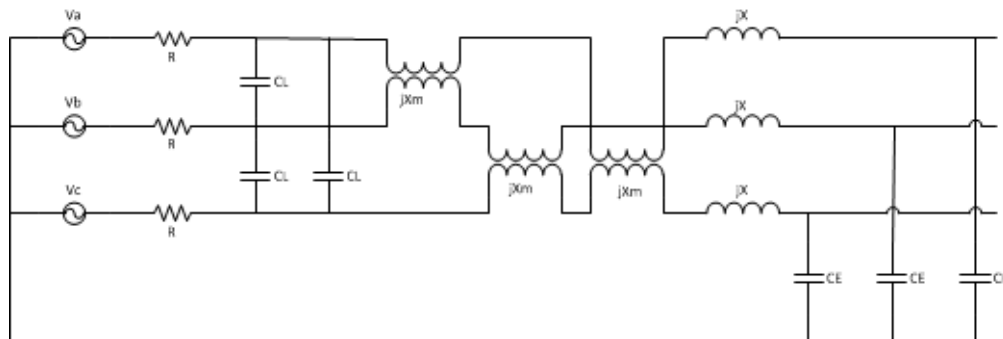


Figure 2. 1: Transmission line model

Figure 2.1 depicts a transmission line model with series resistance R , series-inductance jX , mutual-inductance jX_m , shunt-capacitance C_e and shunt-conductance C_l .

2.1. DIRECT- CURRENT RESISTANCE OF CONDUCTORS

The resistance value of a transmission line conductor is the largest cause of power loss in a transmission line system. If the distribution of current throughout a conductor is uniform, which means direct current is flowing in a homogeneous, round cylindrical wire, the effective resistance of the conductor is equal to the direct current resistance as follows:

$$R_{dc} = \rho \frac{1}{\pi a^2} \text{ ohms/meter} \quad (2.1)$$

where ρ is the resistivity in ohm-meters and a is the conductor radius in meters which together with π represents the conductor area. The value of ρ depends on conductor material [6].

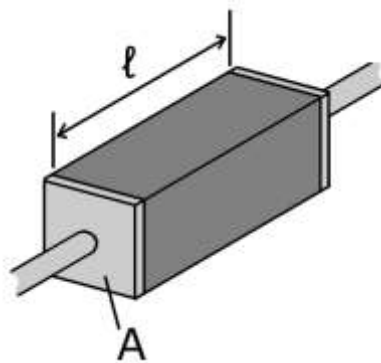


Figure 2. 2: Resistance of a cylindrical conductor [4]

The resistivity of copper at 20 °C typically lies between the values of $\rho_{20} = 1.7241 \cdot 10^{-8}$ and $\rho_{20} = 1.78 \cdot 10^{-8}$ ohm-meters. When temperature changes occur the resistivity of the metal increases proportionately with temperature within the temperature limits encountered in transmission lines. The temperature change is taken into account through the equation

$$\rho = \rho_{20}[1 + \alpha(t - 20)] \quad (2.2)$$

where t is the actual line temperature in °C , and α is the temperature coefficient of the resistance. Hence, with variation in temperature due to geographic or seasonal differences the parameter of resistivity varies.

2.2. INDUCTANCE OF A TRANSMISSION LINE

The familiar concepts of magnetic fields and magnetic induction are applied to calculate the inductive reactance of a transmission line. To obtain accurate values for the inductance of a transmission line, it is essential to take the internal flux as well as the external flux of each conductor into consideration. If an alternating current is flowing in a conductor, a magnetic flux is created within the coil as seen in Figure 2.3. In a one turn coil the number of linkages is equal to the total flux enclosed by the one turn. The effects of the line ends of a transmission line can be neglected, because the length of the line in regards to the line ends accounts for the majority of the inductance characteristics. Additionally, the return path of the conductor can generally be disregarded since it is

assumed to be far away from the conductor and the flux linkages will be very large. Figure 2.4 depicts a solid, round, infinitely long conductor carrying a current of i amperes.

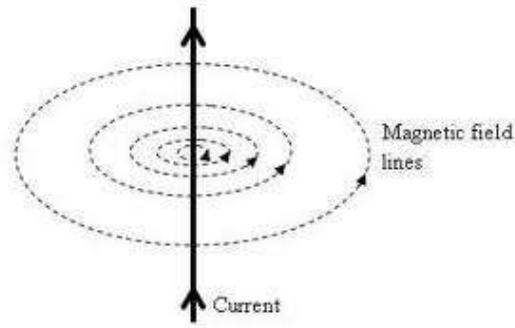


Figure 2. 3: Conductor with external magnetic field [5]

If the current inside the conductor is assumed to be constant (dc), it will be uniformly distributed over the conductor cross section. However, if the current is alternating (ac), then the current density will be larger at the outside of the conductor than at the inside. This phenomenon is called skin effect and is discussed extensively in Chapter 6. In this section the internal-, external-, and total inductances of a solid cylindrical conductor are computed first. Secondly, the flux linkage of several different conductors is computed. Uniform current distribution is assumed in the following scenarios whereas skin effect is discussed in Chapter 6 [7].

Ampere's law states that the integral around a closed path of a conductor of the magnetic field tangent to the direction of the path equals the permeability times the current intercepted by the area within the path as in Equation (2.3).

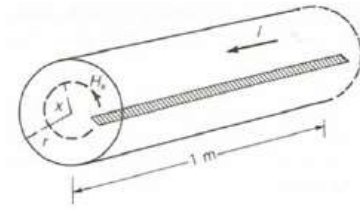


Figure 2. 4: Cross-section of a conductor [2]

H is the magnetic field intensity in Henry, l the distance along the path in meters and $I_{enclosed}$ the enclosed current of the conductor in Ampere. To determine the magnetic field inside a conductor as depicted in Figure 2.4 at radius x , the integral of H_x around the selected contour:

$$\oint H_{tan} dl = I_{enclosed} \quad (2.3)$$

$$H_x = \frac{I_x}{2\pi x} \quad (2.4)$$

Assuming a uniform current distribution within the conductor, Equation (2.4) is modified to:

$$H_x = \frac{Ix}{2\pi r^2} \quad (2.5)$$

For the nonmagnetic conductor, the magnetic flux density B_x is:

$$B_x = \mu_0 H_x = \frac{\mu_0 Ix}{2\pi r^2} \quad (2.6)$$

Differential flux $d\Phi$ per-unit length can be computed in Weber per meter as

$$d\Phi = B_x dx \quad (2.7)$$

Finally, the total flux linkage inside the conductor with integration from 0 to radius r is

$$\lambda_{int} = \int_0^r d\lambda = \frac{\mu_0 I}{2\pi r^4} \int_0^r x^3 dx = \frac{\mu_0 I}{8} \quad (2.8)$$

Internal inductance L_{int} in per-unit length of conductor due to flux linkage is

$$L_{int} = \frac{\lambda_{int}}{I} = \frac{1}{2} \times 10^{-7} \quad (2.9)$$

For the external calculation of the inductance, the entire current of the conductor is enclosed in Ampere's Law and linked by the flux outside the conductor,

$$d\lambda = d\Phi = 2 \times 10^{-7} \frac{I}{x} dx \quad (2.10)$$

The integration between two external points at distances D_1 and D_2 from the conductor center gives the external flux linkage λ_{12} between D_1 and D_2 :

$$\lambda_{12} = \int_{D_1}^{D_2} d\lambda = 2 \times 10^{-7} I \ln \left(\frac{D_2}{D_1} \right) \quad (2.11)$$

The external inductance L_{12} per-unit length due to the flux linkages is then

$$L_{12} = \frac{\lambda_{12}}{I} = 2 \times 10^{-7} \ln \left(\frac{D_2}{D_1} \right) \quad (2.12)$$

The total combined flux is the sum of the internal flux linkage and the external flux linkage from $D_1 = r$ to $D_2 = D$.

$$\lambda_p = \frac{1}{2} \times 10^{-7} I + 2 \times 10^{-7} I \ln \left(\frac{D}{r} \right) \quad (2.13)$$

Equation (2.13) can be simplified to the following:

$$\lambda_p = 2 \times 10^{-7} I \left(\ln e^{1/4} + \ln \left(\frac{D}{r} \right) \right) \quad (2.14)$$

where the radius can also be simplified as:

$$r' = e^{-1/4}r = 0.7788r \quad (2.15)$$

The total inductance L_p with internal and external flux linkages out to the distance D in Henry per meter is:

$$L_p = \frac{\lambda_p}{I} = 2 \times 10^{-7} \left(\ln \left(\frac{D}{r'} \right) \right) \quad (2.16)$$

After this detailed derivation, the impact of the magnetic field of multiple cylindrical conductors on the inductance of a single line conductor can be analyzed and evaluated. When the distance between conductors is much larger than the radius, a valid approximation is made by using D instead of $(D-r)$ or $(D+r)$. The total flux linking a conductor k in an array of M conductors carrying currents that sum up to zero is characterized as follows:

$$\lambda_k = 2 \times 10^{-7} \sum_{m=1}^M I_m \ln \frac{1}{D_{km}} \quad (2.17)$$

2.2.1. Three- Phase Three Wire System

A three-phase three wire line consisting of three solid cylindrical conductors a, b, c each with radius r , and with equal phase spacing D between any two conductors is derived below. To determine the inductance, balanced positive-sequence currents I_a, I_b, I_c are assumed and satisfy the criteria $I_a + I_b + I_c = 0$.

$$\lambda_a = 2 \times 10^{-7} \left(I_a \ln \frac{1}{r'} + I_b \ln \frac{1}{D} + I_c \ln \frac{1}{D} \right) \quad (2.18)$$

$$= 2 \times 10^{-7} \left(I_a \ln \frac{1}{r'} + (I_b + I_c) \ln \frac{1}{D} \right) \quad (2.19)$$

Using the relationship of $(I_b + I_c) = -I_a$,

$$\begin{aligned}\lambda_a &= 2 \times 10^{-7} \left(I_a \ln \frac{1}{r'} - I_a \ln \frac{1}{D} \right) \\ &= 2 \times 10^{-7} I_a \ln \frac{D}{r'}\end{aligned}\tag{2.20}$$

The inductance of phase a then is

$$L_a = \frac{\lambda_a}{I_a} = 2 \times 10^{-7} \ln \frac{D}{r'}\tag{2.21}$$

Since the three-phase wire system ideally is symmetric, the same result is obtained for $L_b = \lambda_b/I_b$ and for $L_c = \lambda_c/I_c$. Only one phase needs to be considered for balanced three-phase operation of the line.

2.2.2. Conductor Stranding

In the following, composite conductors, which consist of two or more solid cylindrical subconductors in parallel, will be analyzed. The assumption of identical conductors and equal current sharing is applied [7].

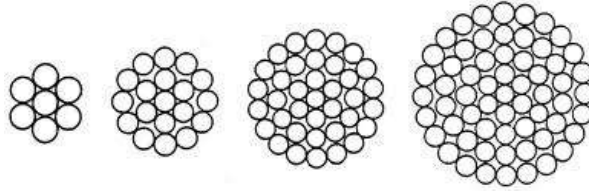


Figure 2. 5: Stranded Conductors [6]

A conductor x has N identical subconductors, each with a radius r_x and with current (I/N) . Conductor y consists of M identical subconductors, each with radius r_y and with return current $(-I/M)$. The inductance of conductor x , $L_x = \frac{\lambda_x}{I}$ can be written as

$$L_x = 2 \times 10^{-7} \ln \frac{D_{xy}}{D_{xx}} \quad (2.22)$$

where

$$D_{xy} = \sqrt[MN]{\prod_{k=1}^N \prod_{m=1'}^M D_{km}} \quad (2.23)$$

and

$$D_{xx} = \sqrt{N^2 \prod_{k=1}^N \prod_{m=1}^N D_{km}} \quad (2.24)$$

D_{xy} is the MN th root of the product of the MN distances from the subconductor x to the subconductors of conductor y . Equally, the same can be achieved for conductor y .

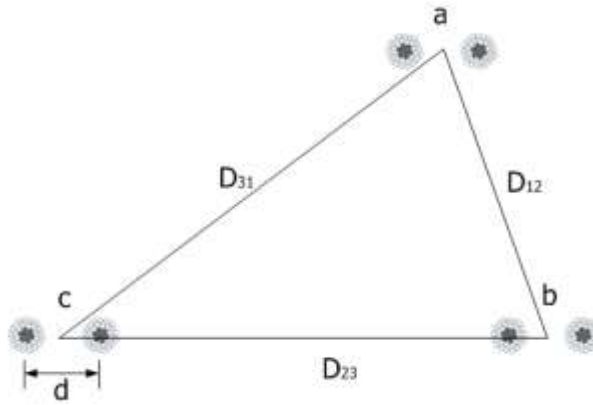


Figure 2. 6: Subconductors of a Transmission Line [2]

D_{xy} is usually called the geometric mean distance (GMD) between conductors x and y .

D_{xx} is called the geometric mean radius (GMR) of the conductor. Values of GMD and GMR are generally provided by manufacturers and exist in various handbooks.

2.2.3. Transposition

If the spacing between conductors is not symmetrically located, unbalanced flux linkages occur, and the phase inductances are unequal. Voltage drops will be different in the different phases of the line. The balance of a three-phase system can be restored by applying the technique of transposition which can be seen in Figure 2.7.

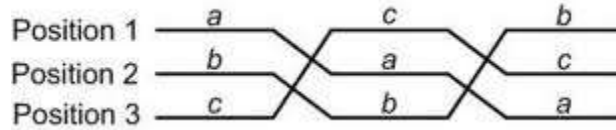


Figure 2. 7: Transposition of phase conductors [2]

Each phase conductor is relocated for one third of the length of the line into every possible position that is occupied by the other conductors. With a length of the entire line, each transposition section will be $1/3$ of the line length. Conductor positions are marked 1, 2, 3 with the distances D_{12} , D_{23} , D_{31} between the conductors. Flux linkage of the phase a conductor in position 1 is

$$\lambda_{a1} = 2 \times 10^{-7} \left(I_a \ln \frac{1}{D_s} + I_b \ln \frac{1}{D_{12}} + I_c \ln \frac{1}{D_{31}} \right) \quad (2.25)$$

The flux linkages of the conductor while it is in the other positions are as follows:

$$\lambda_{a2} = 2 \times 10^{-7} \left(I_a \ln \frac{1}{D_s} + I_b \ln \frac{1}{D_{23}} + I_c \ln \frac{1}{D_{12}} \right) \quad (2.26)$$

Since each single position accounts for a third of the entire conductor, the average of the above flux linkages can be taken

$$\lambda_a = \frac{\lambda_{a1} + \lambda_{a2} + \lambda_{a3}}{3} \quad (2.27)$$

$$= \frac{2 \times 10^{-7}}{3} \left[3I_a \ln \frac{1}{D_s} + I_b \ln \frac{1}{D_{12}D_{23}D_{31}} + I_c \ln \frac{1}{D_{12}D_{23}D_{31}} \right]$$

And simplified using

$$(I_b + I_c) = -I_a \quad (2.28)$$

So that the above equation is simplified to

$$\lambda_a = \frac{2 \times 10^{-7}}{3} \left[3I_a \ln \frac{1}{D_s} - I_a \ln \frac{1}{D_{12}D_{23}D_{31}} \right] \quad (2.29)$$

$$= 2 \times 10^{-7} I_a \ln \frac{\sqrt[3]{D_{12}D_{23}D_{31}}}{D_s}$$

$$L_a = \frac{\lambda_a}{I_a} = 2 \times 10^{-7} \ln \frac{\sqrt[3]{D_{12}D_{23}D_{31}}}{D_s} \quad (2.30)$$

The same result is obtained for L_b and L_c . D_s is the conductor GMR for stranded conductors, or the r' for solid cylindrical conductors.

2.2.4. Bundling

Bundling is the common practice where more than one conductor at voltages above 230kV is used per phase. The electric field strength at the surface of the conductor is reduced. This eliminates or reduces the corona effect and its undesirable side effects such as power loss, communication interference and audible noise [7].

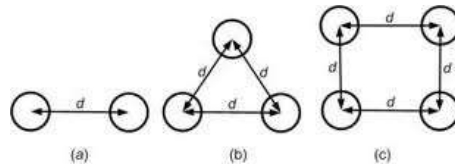


Figure 2. 8: Conductor Bundling [2]

For calculating the inductance of a bundled conductor, D_s is replaced by the *GMR* of the bundle. If a conductor is stranded and the bundle spacing is large in comparison to the conductor outside radius, each stranded conductor is first replaced by an equivalent solid cylindrical conductor with *GMR*. Secondly, the bundle is replaced by one equivalent conductor with $GMR = D_{SL}$.

2.3. CAPACITANCE OF A TRANSMISSION LINE

The capacitance of a transmission line is generated by a potential difference between conductors. It causes conductors to charge in the same way as two plates of a capacitor with a potential difference. Just like the inductive component of transmission lines was calculated based on the basic laws of magnetic fields, now the capacitive components will be calculated based on the basic laws of electric fields. The first step is to compute the electric field of a uniformly charged, solid cylindrical conductor. Gauss's law states that the total electric charge within a closed surface equals the total flux emerging from the surface as in Figure 2.9.

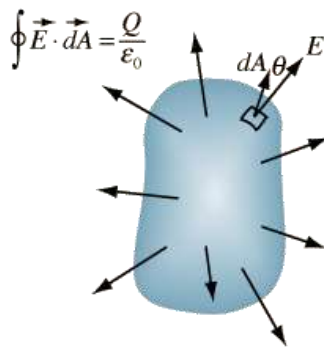


Figure 2. 9: Visualization of Gauss's law [7]

In particular, this describes that the normal component of electric flux density integrated over a closed surface equals the enclosed charges as in Equation (2.30).

$$\oiint D_{\perp} ds = \oiint \epsilon E_{\perp} ds = Q_{enclosed} \quad (2.30)$$

where D_{\perp} is the normal component of electric flux density, E_{\perp} is the normal component of electric field strength, and ds accounts for the differential surface area. ϵ denotes the permittivity of the surrounding medium. An infinitely long, straight, round conductor has the charge q coulombs per meter. It can be regarded solely because it is far removed from other conductors in space. All charges are uniformly distributed on the conductor surface; hence, all the equipotential surfaces around the conductor will be concentric cylinders as in Figure 2.10.

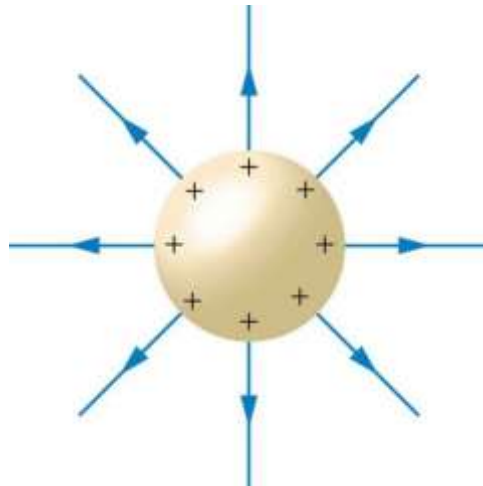


Figure 2. 10: Electric Field of a charged conductor [8]

Inside this perfect conductor, Ohm's law can be applied, stating that the internal electric field is zero. To determine the electric field outside the conductor the radius is

selected larger than the conductor radius. By integrating (2.30) the following equation is obtained for a one meter length:

$$E_x = \frac{q}{2\pi\epsilon x} \quad (2.31)$$

where ϵ is the value of $\epsilon = \epsilon_0 = 8.854 \times 10^{-12} \text{ F/m}$ in free space.

The potential difference between two concentric cylinders at distances D_1 and D_2 from the conductor midpoint can be found from the equation

$$V_{12} = \int_{D_1}^{D_2} E_x dx \quad (2.32)$$

And written as

$$V_{12} = \int_{D_1}^{D_2} \frac{q}{2\pi\epsilon x} dx = \frac{q}{2\pi\epsilon} \ln \frac{D_2}{D_1} \quad (2.33)$$

The result of Equation (2.33) is the voltage between two points at distances D_1 and D_2 from the conductor center. This procedure can be applied to an array of M solid cylindrical conductors. A voltage V_{ki} between an array of M solid cylindrical conductors in respect to the various charges q_m acting on the single conductor from multiple conductors can be expressed via superposition as follows:

$$V_{ki} = \frac{1}{2\pi\epsilon} \sum_{m=1}^M q_m \ln \frac{D_{im}}{D_{km}} \quad (2.34)$$

A single-phase two-wire system with equal phase spacing can now be analyzed to obtain the capacitance value. Conductors are energized by a voltage source so that x contains the positive charge and conductor y contains the equal amount of negative charge, assuming the conservation of energy.

$$V_{xy} = \frac{1}{2\pi\epsilon} \left[q \ln \frac{D_{yx}}{D_{xx}} - q \ln \frac{D_{yy}}{D_{xy}} \right] \quad (2.35)$$

This equation can be simplified using $D_{xy} = D_{yx} = D$, $D_{xx} = r_x$, and $D_{yy} = r_y$ to the following

$$V_{xy} = \frac{q}{\pi\epsilon} \ln \frac{D}{\sqrt{r_x r_y}} = \frac{q}{2\pi\epsilon} \ln \frac{D_{yx} D_{xy}}{D_{xx} D_{yy}} \quad (2.36)$$

Now, for a one meter long line, the capacitance between two conductors is

$$C_{xy} = \frac{q}{V_{xy}} = \frac{\pi\epsilon}{\ln \left(\frac{D}{\sqrt{r_x r_y}} \right)} \quad (2.37)$$

And if the radii of the two conductors are equal $r_x = r_y = r$, the final capacitance is

$$C_{xy} = \frac{\pi\epsilon}{\ln \left(\frac{D}{r} \right)} \quad (2.38)$$

For capacitances to neutral where the voltage to ground is half the size of the provided value the capacitance to neutral needs to be multiplied by the factor of 2. The capacitance from either line to the ground neutral is

$$C_n = C_{xn} = C_{yn} = \frac{q}{V_{xn}} = \frac{2q}{V_{xy}} = \frac{2\pi\epsilon}{\ln \left(\frac{D}{r} \right)} \quad (2.39)$$

2.3.1. Three- Phase Three Wire System

If a three-phase line system is now taken into consideration and the phases are equally spaced apart and the positive sequence charges q_a , q_b , q_c are only taken into consideration so that the sum of all charges amounts to zero such as $q_a + q_b + q_c = 0$.

Then the voltage between two conductors a and b is

$$V_{ab} = \frac{1}{2\pi\epsilon} \left[q_a \ln \frac{D_{ba}}{D_{aa}} + q_b \ln \frac{D_{bb}}{D_{ab}} + q_c \ln \frac{D_{bc}}{D_{ac}} \right] \quad (2.40)$$

Simplifications $D_{aa} = D_{bb} = r$, and $D_{ab} = D_{ba} = D_{ca} = D_{cb} = D$ are made and the equation can be modified to

$$\begin{aligned} V_{ab} &= \frac{1}{2\pi\epsilon} \left[q_a \ln \frac{D}{r} + q_b \ln \frac{r}{D} + q_c \ln \frac{D}{D} \right] \\ &= \frac{1}{2\pi\epsilon} \left[q_a \ln \frac{D}{r} + q_b \ln \frac{r}{D} \right] \end{aligned} \quad (2.41)$$

Voltages V_{ac} , and V_{bc} can be calculated in a similar manner. The third term in Equation (2.41) is zero, because the distance of a to c and b to c are equal. To obtain the capacitance to ground in the three conductor system it is necessary to again modify the line-to-line voltages into line-to-ground voltages. Since the line-to-ground voltage can be expressed as

$$3V_{an} = V_{ab} + V_{ac} \quad (2.42)$$

It is well known that for a balanced three phase system the positive-sequence line-to-line voltage leads the line-to-neutral voltage by 30 degrees and is larger by the factor of $\sqrt{3}$.

Using this background information V_{an} is

$$V_{an} = \frac{1}{3} \left(\frac{1}{2\pi\epsilon} \right) \left[2q_a \ln \frac{D}{r} + (q_b + q_c) \ln \frac{r}{D} \right] \quad (2.43)$$

And with $q_b + q_c = -q_a$ the equation is modified to

$$V_{an} = \frac{1}{2\pi\epsilon} q_a \ln \frac{D}{r} \quad (2.44)$$

And the capacitance-to-neutral per line length is

$$C_{an} = \frac{q_a}{V_{an}} = \frac{2\pi\epsilon}{\ln\left(\frac{D}{r}\right)} \quad (2.45)$$

Because of symmetry, the same result is obtained for capacitances C_{bn} and C_{cn} .

2.3.2. Conductor Stranding and Transposition

It is common practice to replace a stranded conductor by a perfectly conducting cylindrical conductor. Errors due to this assumption are fairly small and can be neglected.

In an unbalanced conductor system unbalanced line-to-neutral voltages occur. The same approach as mentioned for the inductive components is used to restore a balanced system.

The method of transposition, where each phase conductor occupies each position for a third of the line is applied. The capacitance results to

$$C_{an} = \frac{2\pi\epsilon}{\ln\left(\frac{D_{eq}}{r}\right)} \quad (2.46)$$

where $D_{eq} = \sqrt[3]{D_{ab}D_{bc}D_{ac}}$. This reestablishes the balanced system and simplifies the calculation of the unequally distributed lines.

2.3.3. Bundling

For a bundled conductor system the assumptions of balanced positive sequence charges, equally shared charges, and much larger phase spacing than bundle spacing are applied to simplify the mathematical procedure to calculate the capacitances. With these simplifications and a transposed line, the derivation of the capacitance value yields

$$C_{an} = \frac{2\pi\epsilon}{\ln\left(\frac{D_{eq}}{D_{SC}}\right)} \quad (2.46)$$

where $D_{SC} = \sqrt{rd}$ is the equation for a two-conductor bundle. It is modified for three- or four- conductor bundles. This procedure is very similar to the approach for inductive components and depicts the same simplifications to a geometric mean radius D_{SC} .

2.4. SHORT, MEDIUM AND LONG LINES

This section will give a brief introduction and overview of the different approaches for short, medium and long transmission lines. A simplification in the treatment of transmission lines is applied, which reduces the mathematical complexity to calculate the line parameters and the resulting impact on voltages and currents. The three phase system is reduced to an equivalent single-phase system where the terminal conditions of both ends of the line will relate to each other in the form of

$$V_s = AV_R + BI_R \tag{2.48}$$

$$I_s = CV_R + DI_R \tag{2.49}$$

or

$$\begin{bmatrix} V_s \\ I_s \end{bmatrix} = \begin{bmatrix} A & B \\ C & D \end{bmatrix} \begin{bmatrix} V_R \\ I_R \end{bmatrix} \tag{2.50}$$

where V_s and I_s are the sending-end voltages and current, and V_R and I_R are the receiving-end voltage and current. The parameters A , B , C , and D are complex numbers that are derived from the line parameters R , L , C , and G . The short transmission line method is usually used for overhead 60-Hz lines less than 80 km long. Shunt admittance is neglected and only series components like resistance and reactance are included into the calculation as depicted in Figure 2.11.

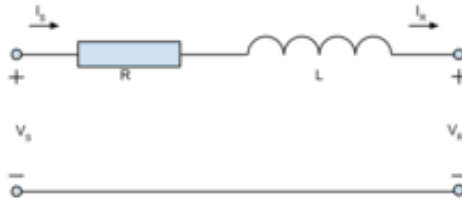


Figure 2. 11: Short- Line Model [9]

For an entirely transposed three-phase system, Z is the series impedance of the system, and Y is the shunt admittance

$$z = R + j\omega L \tag{2.51}$$

$$y = G + j\omega C \tag{2.52}$$

$$Z = zl \tag{2.53}$$

$$Y = yl \tag{2.54}$$

Since the shunt component can be neglected in short lines, the matrix is modified to

$$\begin{bmatrix} V_s \\ I_s \end{bmatrix} = \begin{bmatrix} 1 & Z \\ 0 & 1 \end{bmatrix} \begin{bmatrix} V_R \\ I_R \end{bmatrix} \tag{2.55}$$

Medium-length lines typically range from 80 to 250 km at 60 Hz. In this procedure the shunt admittance is used and divided to contribute half on each side, the line beginning and the line end as shown in Figure 2.12.

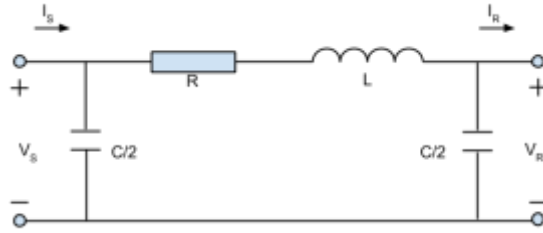


Figure 2. 12: Medium- Length Line Model [9]

This electrical circuit model is called the nominal π circuit. Based on the below KVL (2.56) and KCL (2.57) equations with a few simplifications

$$V_s = V_R + Z \left(I_R + \frac{V_R Y}{2} \right) \quad (2.56)$$

$$I_s = I_R + \frac{V_R Y}{2} + \frac{V_s Y}{2} \quad (2.57)$$

the matrix can be formulated as

$$\begin{bmatrix} V_s \\ I_s \end{bmatrix} = \begin{bmatrix} \left(1 + \frac{YZ}{2} \right) & Z \\ Y \left(1 + \frac{YZ}{4} \right) & \left(1 + \frac{YZ}{2} \right) \end{bmatrix} \begin{bmatrix} V_R \\ I_R \end{bmatrix} \quad (2.58)$$

The procedure to calculate the matrix components of the long transmission line shall not be derived but simply be mentioned and depicted in this paragraph. Hyperbolic functions *cosh* and *sinh* are used to characterize the behavior at any given point in the long transmission line. The equations are

$$V(x) = \cosh(yx)V_R + Z_c \sinh(yx)I_R \quad (2.59)$$

$$I(x) = \left(\frac{1}{Z_c} \right) \sinh(yx) V_R + \cosh(yx)I_R \quad (2.60)$$

and the matrix at the total length l turns out to be

$$\begin{bmatrix} V(l) \\ I(l) \end{bmatrix} = \begin{bmatrix} \cosh(\gamma l) & Z_c \sinh(\gamma l) \\ \frac{1}{Z_c} \sinh(\gamma l) & \cosh(\gamma l) \end{bmatrix} \begin{bmatrix} V_R \\ I_R \end{bmatrix} \quad (2.61)$$

Where γ is the propagation constant in $\gamma = \sqrt{zy} \text{ m}^{-1}$ and Z_c is the characteristic impedance $Z_c = \sqrt{\frac{z}{y}}$, whose units are Ω . A similar structure to the nominal π can be implemented called the equivalent π . This procedure is used for long transmission lines based on circuit representation. It is a slightly modified version of the medium length nominal π version, where Z' and Y' are used instead of Z and Y .

$$Z' = Z_c \sinh(\gamma l) \quad (2.62)$$

$$\frac{Y'}{2} = \frac{\tanh(\frac{\gamma l}{2})}{Z_c} \quad (2.63)$$

The derivation of line parameters and transmission line models depicts the various assumptions and simplifications of line parameter calculation. Further work for in depth analysis of the grounding of shield wire assumption and skin effect can be performed hereafter.

3. IMPACTS ON LINE PARAMETERS

Line parameter calculation of transmission lines is a widely known and common procedure in the field of power engineering. The approaches are generally accepted. However, new technological advancements in the power industry lead to the necessity for review and reevaluation of these methods. Simplifying assumptions do not hold true due to varying load, fault resistance, remote infeed and zero-sequence mutual coupling in parallel transmission lines. Accuracy of line parameters, particularly zero- sequence line impedance is subject to many uncertainties. This stems from the fact that zero-sequence line impedance depends on earth resistivity along with tower grounding impedances, which tend to be estimated in common calculation techniques. This example illustrates the complexity and necessity for a closer look at the procedure of line parameter calculation [2]. In the following chapter, assumptions and simplifications in the procession of line parameter calculation are overviewed and described to give a general idea of the challenges and possibilities for further improvement of line parameter calculation.

3.1. VARYING EARTH RESISTIVITY

Earth resistivity ρ is commonly known as the factor that impacts the current flow through the earth. This electrical factor is depended on the type of soil that the transmission line and earth return current is operating in. Determining the exact value of this parameter is difficult since it varies greatly with soil type, moisture content and temperature. This variation in earth resistivity severely affects the zero-sequence line impedance which

increases asymptotically with increase in earth resistivity [3]. The value of earth resistivity varies largely and can take any value between 50 to 8000 Ωm which points out the importance to know the value for the earth resistivity.

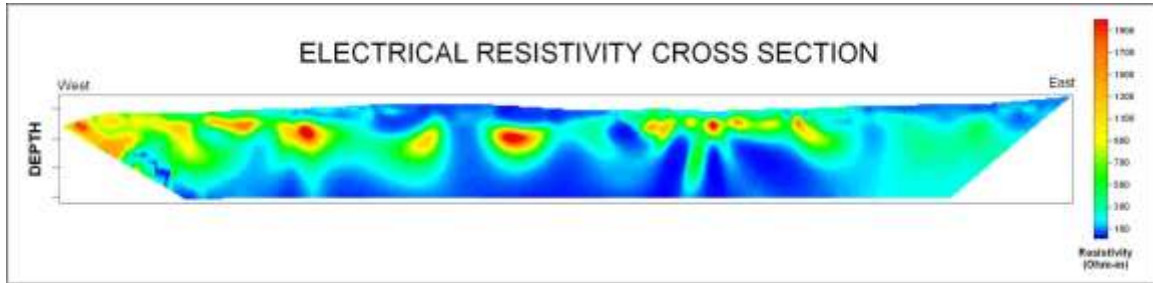


Figure 3. 1: Resistivity across various earth sections [12]

A standardized, homogeneous value of 100 Ωm is commonly used when the exact consistency of the earth is not known. The amount of moisture in the soil additionally plays a role in the choosing of the earth resistivity. On a dry and sunny day the soil has a higher resistivity than on a rainy day. Zero-sequence components in the transmission line model are largely impacted by the earth resistivity value. In addition to the assumption of soil resistivity the soil surface is simplified to a plane surface. Geographical conditions are not taken into consideration in the calculation of line parameters and are largely simplified.

A mountain range or hilly area as depicted in Figure 3.2 where the distance to ground varies, is not taken into consideration in the overall line parameter calculation of the model. For further detail on this topic the reference document is [3].

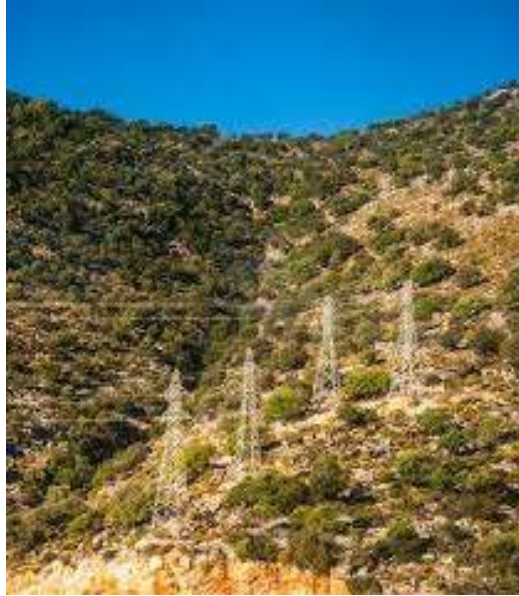


Figure 3. 2: Transmission line on a hill

3.2. VARYING TRANSPOSITION OF THE LINE

Line transposition is the physical change in location of a phase conductor at periodic intervals. This procedure is conducted to balance the magnetic and electric fields of the conductors. In a three phase system these rotations ideally occur every one-third of the total line length. In a completely transposed and then ideally balanced system as analyzed in Equation (2.29), the off-diagonal elements of the sequence matrix are zero, whereas the diagonal elements are the zero-, positive-, and negative- sequence components. Many

transmission lines are not transposed in reality and hence the assumption of line transposition is flawed.

Line parameters computed with transposition do not match the actual values in a non-transposed system. Additionally, many times the transposition is not at exactly one third of the line length, but varies slightly. Transmission lines may not be transposed due to increased costs and design considerations. In such a case, actual line impedance will be different than that obtained by the transposition assumption and will affect accuracy of both one- and two-terminal fault location methods. Increase in error is however marginal, around 0.4 % [3].

3.3. VARYING LENGTH OF THE TRANSMISSION LINE

The assumption of ideal horizontal and parallel transmission lines largely neglects the effect of dips in wires and the circumstances of not ideally parallel wires to one another.

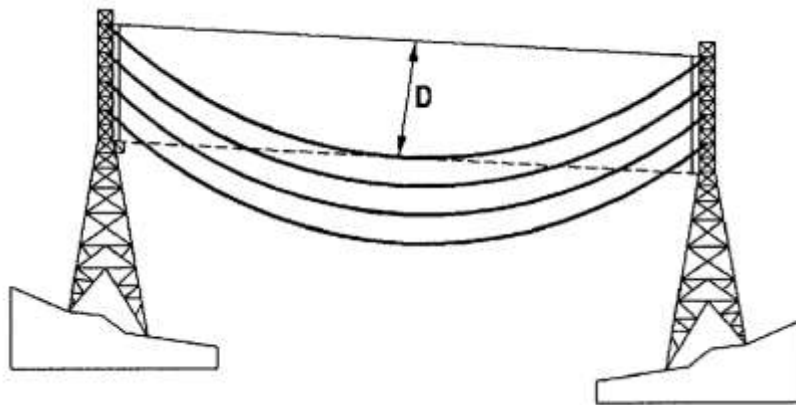


Figure 3. 3: Dip in Transmission Line [13]

In reality multiple strands of wires going into different directions and intersecting with each other on a long transmission line exist. The original lines might be close to parallel, but off by some small factor. Load conditions and temperatures impact the characteristics of line parameters. High temperatures let the line material expand and hence create a larger dip between towers than commonly anticipated. Meteorological conditions such as the seasonal changes of summer and winter impact the dips of the lines.

If the conductor consists of multiple strands, the effective d-c resistance will be slightly increased than is calculated from the total conductor length and cross section of the conductor. This is due to the fact that alternate layers of wire of a stranded conductor are spiraled in opposite directions to prevent unwinding and to make the outer radius of one layer coincide with the inner radius of the next layer. Spiraling makes the strands 1 or 2% longer than the actual conductor length. As a result, the dc resistance of a stranded conductor is 1 or 2% larger. Additionally, this technique enhances the flexibility of the wire.



Figure 3. 4: Spiraling of a Conductor [2]

The assumption of uniformly distributed current throughout the cross section of the conductor will be analyzed at a later time in this thesis. While the assumption is physically correct for a homogeneous conductor and direct current, it needs to be slightly adjusted and modified for alternating current.

3.4. CARSON'S MODEL

For an entire three-phase overhead line system, the earth surface underneath the conductors is assumed as a perfectly conducting horizontal plane, even if the earth terrain is irregular. A method where the conductor at a particular height above a perfectly conducting plane is positively charged and induces an equal amount of negative charges on the earth is used. If neutral conductors where no current is flowing through in balanced conditions are also present and shall be taken into consideration, the earth return conductor can be replaced by a simulated earth return conductor underneath the ground as depicted in Figure 3.5. Only if the phase currents are unbalanced, there may be a return current in the grounded neutral wires and in the earth. In this case, the return current seeks the lowest impedance return path. Hence, the return current largely depends on the condition of the grounding and earth material, moisture or resistivity of the ground.

This approach is based on the Carson's equations, which concludes that the earth can be replaced by a set of "earth return" conductors that are located at the same distance underneath the ground. Line constants are generally calculated using Carson's equations and the Kron reduction method [4] [3] [5]. The full Carson's model uses a method of images wherein every conductor above the ground has a fictitious image conductor at the same distance below the ground, as shown in Figure 3.5.

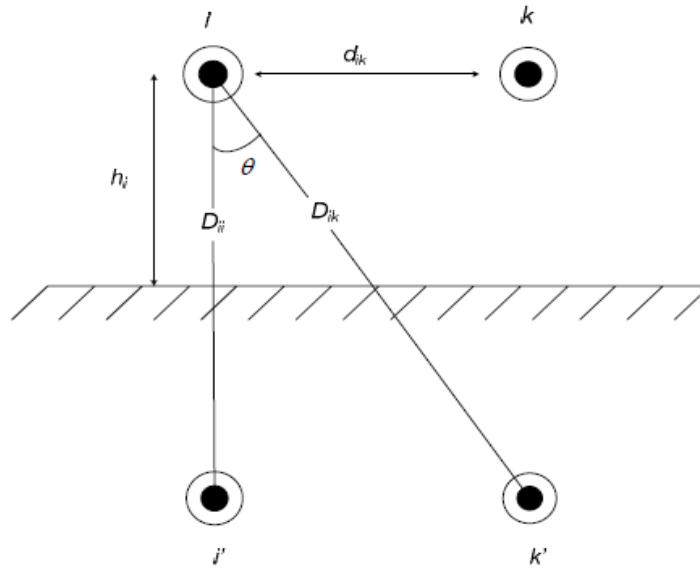


Figure 3. 5: Earth- return conductors underneath ground [11]

This approach highly simplifies the procedure to calculate the line inductance and taking the neutral wires into account.

3.5. KRON REDUCTION

A primitive impedance matrix as in Equation 2.1 is constructed to represent the overall line parameters and characteristics of a transmission line, where i and k refer to phase conductors and n is the neutral conductor. In theoretical approaches the neutral conductor is assumed to be perfectly grounded, otherwise the Kron reduction method cannot be applied. Figure 3.5 illustrates a three-phase four wire system with this assumption [5]. Line to ground voltages are depicted as V_{ag} , V_{bg} and V_{cg} , phase currents as I_a , I_b , I_c and neutral current as I_n .

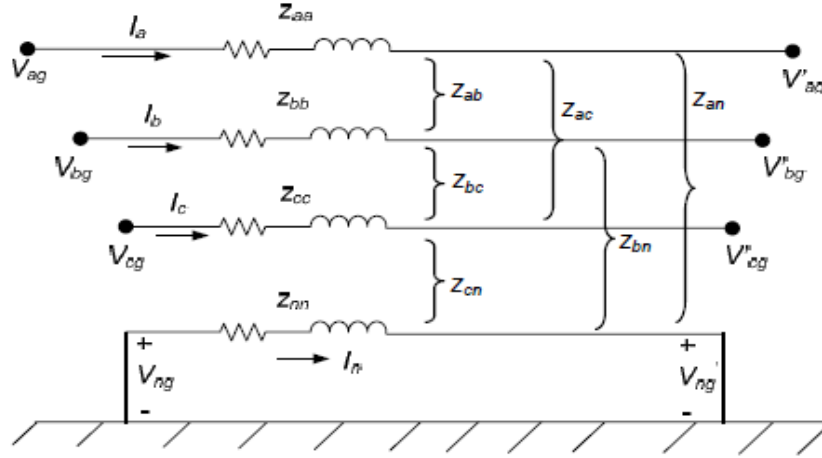


Figure 3. 6: 4- Wire Transmission System [11]

$$Z_{primitive} = \begin{bmatrix} [Z_{ik}] & [Z_{in}] \\ [Z_{nk}] & [Z_{nn}] \end{bmatrix} \quad (3.1)$$

A grounded neutral conductor has its voltages at earth potential and hence is equal to zero. This assumption leads to the simplification to generate a matrix with a 3 by 3 system and a potential creation of the sequence components, if the matrix can be assumed to be transposed. To obtain a phase impedance matrix and the corresponding sequence impedances, the Kron reduction as in Equation (3.2) is applied to the primitive impedance matrix in (3.1).

$$Z_{abc} = [Z_{ik}] - [Z_{ik}] \times [Z_{ik}]^{-1} \times [Z_{ik}] \Omega/mile \quad (3.2)$$

In practice, however, shield wires are grounded to the earth through a finite tower footing resistance. This particular assumption of grounded shield wire is discussed in detail in Chapter 4.

4. ASSUMPTIONS IN FAULT LOCATION ALGORITHMS

Fault location algorithms make certain simplifying assumptions when estimating the distance to a fault on the transmission grid. Accuracy is affected when these simplifying assumptions do not hold true due to, for example, loading, fault resistance, remote infeed or zero-sequence mutual coupling in parallel transmission lines. Additionally, these algorithms require the input of voltage and current phasors during the fault as well as line impedance parameters to obtain a location estimate. Inaccuracy in these input parameters further adds to the error in fault location. The phenomenon of grounded shield wire assumption in transmission lines is analyzed in this chapter.

4.1. FAULT LOCATION ALGORITHMS

One- and two- ended impedance-based fault location algorithms are commonly used to locate faults in a networked transmission system so as to expedite service restoration and improve service reliability. One- ended methods need voltage and current measurements, captured by intelligent electronic devices during the fault, at one-end of the line while two- ended methods need voltages and currents from both ends of the line. When the line impedance to the fault is known the actual distance to the fault can easily be calculated. One-ended methods are popular because they do not require any communication channel or synchronized measurements. They are used in many commercial distance relays. However, these methods require the knowledge of the fault type as well as the positive- and zero-sequence impedance of the transmission line. Two-ended methods use voltage and current phasors from both sides of a transmission line and do not require zero-

sequence components. For a detailed analysis and explanation of FLA methods, refer to [3].

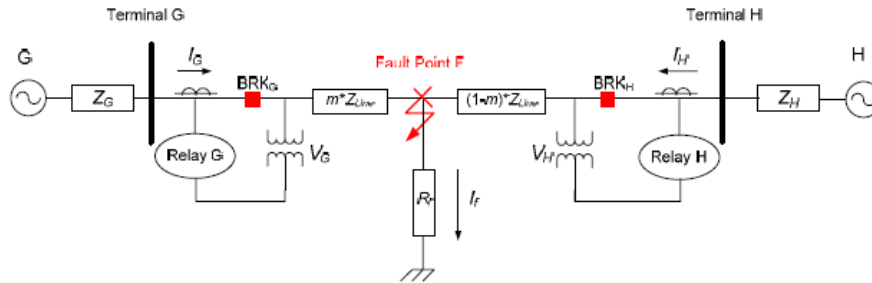


Figure 4. 1: Fault- Locating Mechanism [11]

4.2. GROUNDING OF SHIELD WIRE ASSUMPTION

Positive- and zero-sequence impedances of a transmission line are generally calculated by assuming that the shield wires are directly grounded to the earth. In practice, however, the shield wires are grounded through a finite tower footing resistance. Since calculated line impedances are different from actual values, this chapter investigates the effect of the grounded shield wire assumption on the accuracy of fault location estimates.

Line constants are generally calculated using Carson's equations and the Kron reduction method [4]. The neutral conductor is assumed to be perfectly grounded to the earth. In practice, however, shield wires are grounded to the earth through a finite tower footing resistance which has a value between 5 and 100 ohms. This is shown for a single circuit transmission line having one ground wire in Figure 4.2.

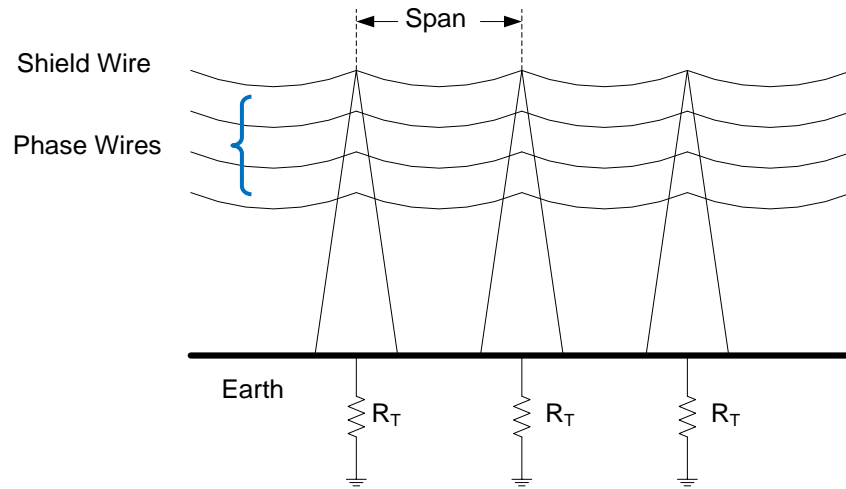


Figure 4. 2: Shield Wire Grounded through a Finite Value of Tower Footing Resistance [11]

In Figure 4.2, ‘span’ is the length of the transmission line segment between two adjacent towers and R_T is the tower footing resistance. Since the neutral is no longer at the earth ground potential, line impedances calculated using the Kron reduction will be different from actual line parameters and lead to inaccurate fault location estimates. For this reason, this section evaluates the impact of the grounded shield wire assumption on the accuracy of fault location algorithms.

4.2.1. Benchmark Test Case: 69-kV Single Circuit Transmission Line

To analyze the impact of tower footing resistance on the accuracy of fault location algorithms, the test case adopted herein is one of the example circuits described in IEEE C37.114 [1]. The simple topology of the feeder and availability of complete network data makes the example circuit a useful benchmark. The test case was modeled in the time-domain using PSCAD simulation software [6]. It is used to simulate short-circuit

faults occurring on transmission lines and generate voltage and current waveforms during the fault event. The single line diagram of the test system is shown in Figure 4.3.

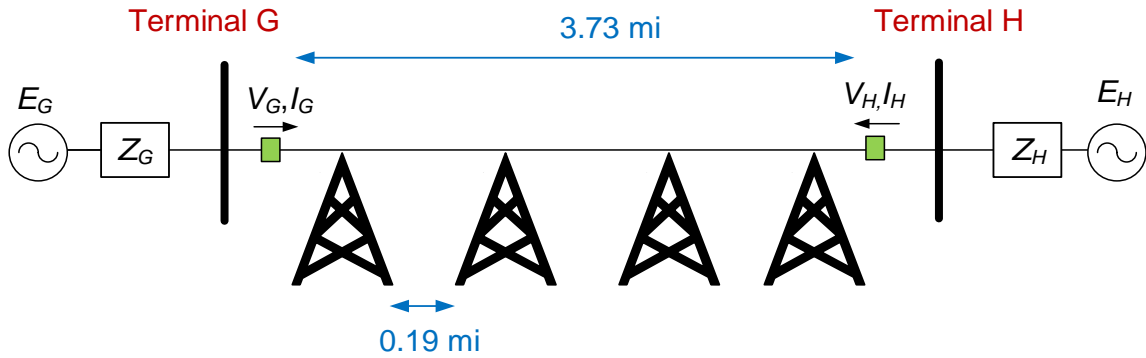


Figure 4. 3: 69-kV Single circuit Transmission Line Test Case [11]

In the figure, V_G and I_G are the voltage and current waveforms recorded at terminal G while V_H and I_H are the voltage and current waveforms recorded at terminal H. The rated voltage at both the terminals is 69 kV. The network upstream from terminal G is represented by a Thevenin equivalent voltage source E_G and equivalent impedance Z_G . Similarly, the Thevenin equivalent voltage and impedance at terminal H is denoted by E_H and Z_H , respectively.

Value of these parameters are obtained from [1] and listed below:

$$Z_{G1} = 3.75 \angle 86^\circ \Omega \quad Z_{H1} = 12 \angle 80^\circ \Omega \quad E_G = 1.0 \angle 10^\circ \text{ pu}$$

$$Z_{G0} = 11.25 \angle 86^\circ \Omega \quad Z_{H0} = 36.0 \angle 80^\circ \Omega \quad E_H = 1.0 \angle 0^\circ \text{ pu}$$

The voltage source E_G leads E_H by a power angle of 10° which accounts for the net load served by the transmission line. The transmission line is 3.73 miles long and supported by transmission towers every 0.19 miles. Arrangement of the phase and neutral conductors are shown in Figure 4.4 and the description of the material used to build the conductors are given in Table 4.1.

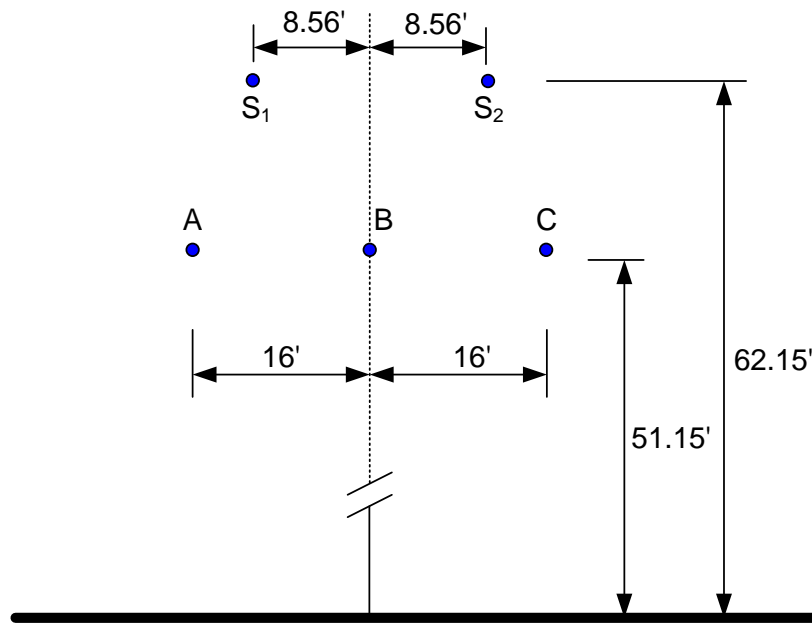


Figure 4. 4: Overhead Line Spacing in Feet [10]

Table 4. 1: Conductor Data

	Material	Resistance (Ω /mile)	Diameter (inch)	Geometric Mean Radius (feet)
Phase conductor	397,500 26/7 ACSR	0.2537	0.7836	0.0265
Shield wire	3/8 A HSS	5.6500	0.3600	0.0120

Since the objective is to investigate the effect of tower grounding resistances on the accuracy of fault location algorithms, the transmission line is modeled in details as an n -phase model and the tower footing resistances are modeled explicitly as shown in Figure 4.5.

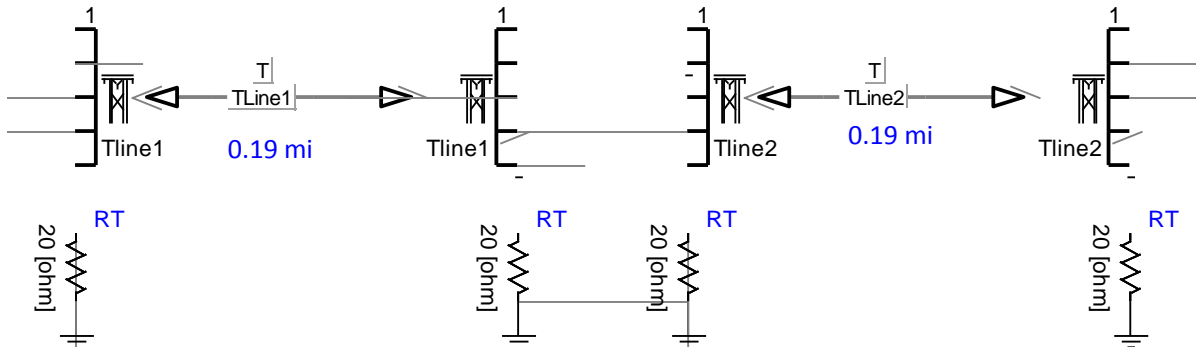


Figure 4. 5: Transmission Line Modeled as an n -phase Model in PSCAD with Two Shield Wires Grounded through a Tower Footing Resistance R_T

Using an earth resistivity value of $100 \Omega\text{m}$ at a system frequency of 60 Hz and assuming that $R_T = 0 \Omega$, the total positive- and zero-sequence impedances of the line are $Z_{Line,1} = 0.95 + j3.11 \Omega$ and $Z_{Line,0} = 3.12 + j8.96 \Omega$, respectively. Note that these line impedances are different from those used in [1].

4.2.2. Impact on the Accuracy of Fault Location Algorithms

The 69-kV benchmark test case was used to analyze the effect of tower grounding on the accuracy of fault location algorithms. The tower footing resistance at every tower was varied discretely at the following values: 0 Ω , 5 Ω , 20 Ω and 100 Ω . Single line-to-ground faults were simulated at 0.75 mi, 1.86 mi, and 2.80 mi to investigate whether the number of tower footing resistances between the monitoring location and the fault play a significant role on the result. Additionally, the angle between source voltages, and the source impedances were varied. Figure 4.6 depicts the impact of varying tower grounding resistances on distance to fault estimates from the Eriksson method [9].

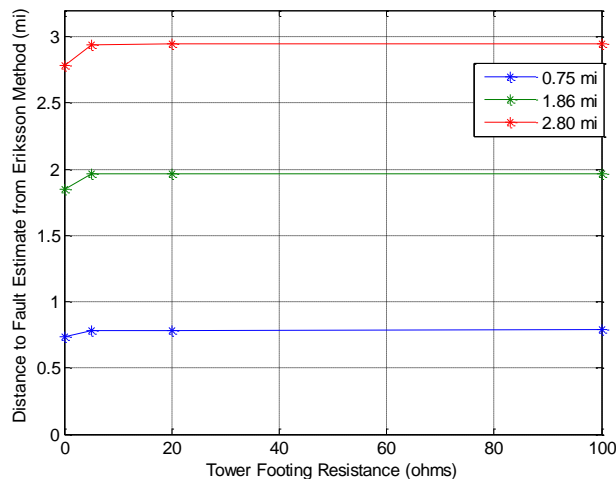


Figure 4. 6: Estimates from Eriksson Method. Tower Footing Resistance = 0 Ω indicates that the tower is grounded directly

As seen from Table 4.2, when the tower footing resistance is 0 Ω , estimates from this method are accurate. The error percentage of 0.17 to 0.33% corresponds to a location error of around 0.01 miles, which is not significant.

Table 4. 2: Impact of Tower Footing Resistance on the Eriksson Method

Actual Distance to Fault (mi)	Error in Fault Location (%)			
	$R_T = 0 \Omega$	$R_T = 5 \Omega$	$R_T = 20 \Omega$	$R_T = 100 \Omega$
0.75	-0.17	1.00	1.00	1.17
1.86	-0.33	2.67	2.67	2.67
2.80	-0.33	3.83	4.00	4.00

Equation (4.1) was used to calculate the error percentages and the negative sign indicates that the location is underestimated.

$$Error \% = \frac{Estimate - Actual}{Total Line Length} \times 100 \quad (4.1)$$

When the tower footing resistance has a value greater than zero, however, error in fault location increases. The magnitude of the error percentage depends on how far the fault is from the monitoring location rather than on the value of the tower footing resistance as seen in Table 4.2. Fault location error from the one-ended methods can be explained by the fact that the tower footing resistance affects the value of the zero-sequence line impedance as shown in Figure 4.7. The positive-sequence impedance of the line remains unchanged. The negative-sequence impedance of the line also remains unchanged since in a transmission line, the positive- and negative-sequence impedances are equal.

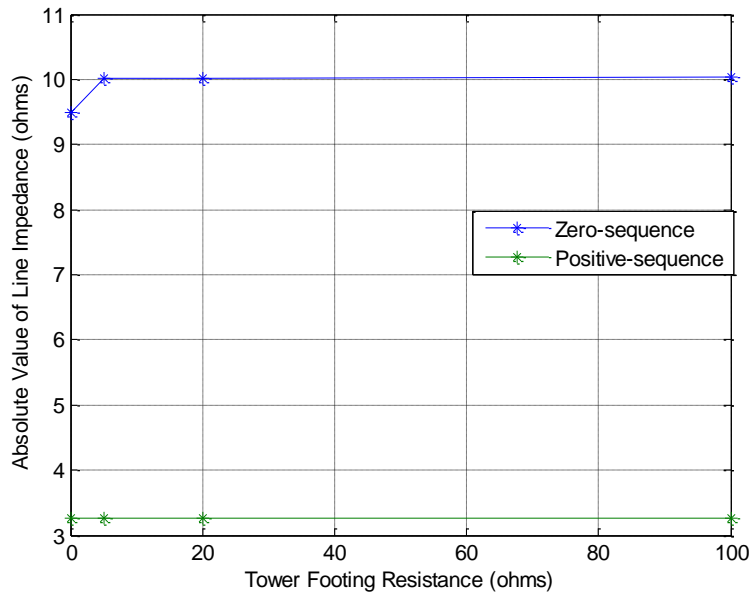


Figure 4. 7: Effect of Tower Footing Resistance on Sequence Line Impedances. Tower Footing Resistance Affects the Zero-sequence Line Impedance Only.

Note that the impedance scan function block in PSCAD [8] was used to calculate the sequence line impedances at different values of tower footing resistance as illustrated in Figure 4.8. This block is a powerful feature of PSCAD and generates the equivalent impedance matrix as seen from the interface point.

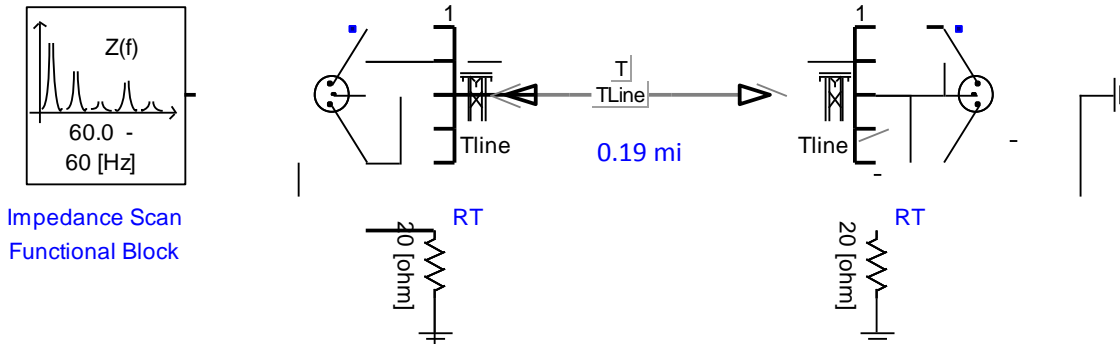


Figure 4. 8: Impedance Scan Function Used in PSCAD to Calculate the Zero-sequence Impedance of the Transmission Line at Different Values of Tower Footing Resistance

Distance to fault estimates from the two-ended unsynchronized negative-sequence method are shown in Figure 4.9 and Table 4.3. Accuracy of this method is not affected by the presence of tower footing resistance. This is because two-ended methods do not use zero-sequence line impedance in their fault location computation.

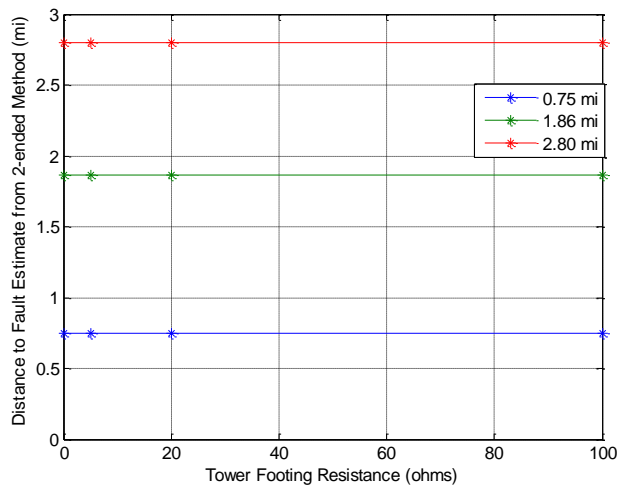


Figure 4. 9: Tower Grounding Resistance Has no Impact on the Accuracy of Two-ended Eriksson Method

Table 4. 3: Estimates from the Two-ended Unsynchronized Two-ended Method

Actual Distance to Fault (mi)	Fault Location Estimates (mi)			
	$R_T = 0 \Omega$	$R_T = 5 \Omega$	$R_T = 20 \Omega$	$R_T = 100 \Omega$
0.75	0.75	0.75	0.75	0.75
1.86	1.86	1.86	1.86	1.86
2.80	2.80	2.80	2.80	2.80

The analysis described above leads to the conclusion that tower footing resistance affects the zero-sequence line impedance only. Since one-ended methods require the input of zero-sequence line impedance to estimate the location of single line-to-ground or double line-to-ground faults, the accuracy of these methods are affected by the presence of a tower footing resistance. The increase in error is around 4%. The analysis also concludes that the size of the tower footing resistance, whether 5 or 100 Ω , has a marginal impact on fault location algorithms. This is because an increase in the tower footing resistance only slightly changes the value of the zero-sequence line impedance. The number of towers between the monitoring location and the fault also does not seem to have a significant impact on the accuracy of one-ended methods. In contrast, two-ended methods are robust to the presence of the tower footing resistance since they do not use zero-sequence line impedance in fault location computation.

5. FREQUENCY VARIATION IN THE TRANSMISSION LINE

The previously made assumption of a uniform current distribution over the cross section of a conductor is incorrect for alternating current, while the assumption is physically correct for a homogeneous conductor with direct current. The detailed analysis of transmission lines where 50 Hz or 60 Hz are most common requires a closer analysis of a phenomenon called skin effect which will be discussed in more detail in the following chapter. Past calculations have largely neglected the presents of skin effect and used the valid assumption of direct current in the conductor because the additional mathematical procedure for a simple line parameter calculation would have been very extensive and involving. With new technologies and software that provide a large amount of computational power a reevaluation of the necessity for a skin effect calculation and implementation into the programs is performed and analyzed in this part of the thesis.

5.1 SKIN EFFECT

An alternating current is flowing through the conductor and magnetic flux is present inside of the conductor. This flux consists of flux lines which are concentric circles with the conductor surface. Centrally located portions of the conductor have larger total flux linkages than do portions that are located close to the outside surface. This brings along the phenomenon that with ac current in the conductor more voltage is induced longitudinally in the inside of the conductor, close to the axis, than on the outside, close to the surface [10]. The overall voltage gradient over the conductor must remain the same in the conductor whether it is measured along the axis in the center or in the area close to

the surface of the conductor. Consequently, the current will be distributed unequally over the cross section and the current density will increase toward the surface as is depicted in Figure 5.1.

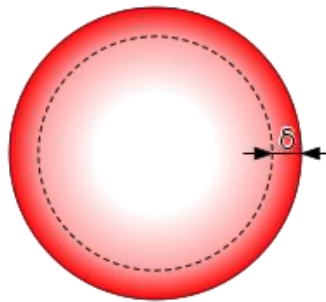


Figure 5. 1: Visualization of Skin Effect [18]

Due to the fact that the ohmic voltage drop is proportional to the current density, it becomes larger close to the surface than close to the axis, compensating for the opposite variation of the induced voltage and restoring the uniformly distributed voltage change over the conductor filaments. The ohmic and induced voltages are out of phase with each other and therefore a variation not only in magnitude of the current density, but also a variation in their phase angles can be expected. This phenomenon is known as skin effect. The mathematical procedure originally performed by Heaviside and Kelvin and an approach and analysis to the implementation of skin effect into the standardized formulas will be given in brief in the following. The detailed procedure can be researched in [10] and [11]. The assumption of a distant return path of the wire as well as complete rotational symmetry of the electric and magnetic fields is entailed in the following mathematical treatment. Current density s in A/m^2 and the electric field intensity K in

volts/meter are purely longitudinal, whereas the magnetic field intensity H is purely tangential. Based on this symmetry conditions and the assumption of nonmagnetic material, Maxwell's differential equations become (in terms of cylindrical coordinates x , z and ϕ):

$$\frac{\partial K}{\partial x} = \mu_0 \frac{\partial H}{\partial t} \quad (5.1)$$

$$\frac{1}{x} \frac{\partial}{\partial x} (xH) = s \quad (5.2)$$

Differentiating the second equation with respect to time and substituting $\frac{\partial H}{\partial t}$ from the first equation yields

$$\frac{1}{\mu_0} \frac{1}{x} \frac{\partial}{\partial x} \left(x \frac{\partial K}{\partial x} \right) = \frac{\partial s}{\partial t} \quad (5.3)$$

And from Ohm's law

$$K = \rho s \quad (5.4)$$

with ρ being the constant resistivity of the conductor material. The substitution of Equation (5.4) into Equation (5.3) and differentiating leads to the result

$$\frac{\partial^2 s}{\partial x^2} + \frac{1}{x} \frac{\partial s}{\partial x} - \frac{\mu_0}{\rho} \frac{\partial s}{\partial t} = 0 \quad (5.5)$$

since only the ac steady-state conditions are studied here. Complex number representation for the current density is used:

$$s(x, t) = \sqrt{2} \operatorname{Re} \{ s(x) e^{j\omega t} \} \quad (5.6)$$

where

$$s(x) = S(x)e^{j\psi(x)} \quad (5.7)$$

$S(x)$ is the RMS amplitude of the current density and $\psi(x)$ its phase angle at distance x from the axis of the conductor. Implementing these terms into the previous Equation (5.5) becomes

$$\frac{\partial^2 s(x)}{\partial x^2} + \frac{1}{x} \frac{\partial s(x)}{\partial x} - \frac{\omega\mu_0}{\rho} s(x) = 0 \quad (5.8)$$

This differential equation determines the variation of complex current density between the axis ($x=0$) and the surface of the conductor. The equation is commonly known as Bessel's differential equation of zero order and has a general solution of

$$s(x) = AJ_0(kx) + BY_0(kx) \quad (5.9)$$

where A and B are arbitrary constants, $J_0(kx)$ and $Y_0(kx)$ are Bessel functions of zero order as well as first and second kinds. Mathematically simplified, the Bessel function $J_0(kx)$ is a transcendental function and is defined by an infinite power series:

$$J_0(kx) = 1 - \frac{k^2 x^2}{2^2} + \frac{k^4 x^4}{2^4 (2!)^2} - \frac{k^6 x^6}{2^6 (3!)^2} + \frac{k^8 x^8}{2^8 (4!)^2} - \dots \quad (5.10)$$

, where the series is uniformly convergent for all finite values of kx real or complex. If the current density at distance x from the axis of the conductor is $s(x)$, then the total current within a cylindrical shell of radius x and thickness dx will be $s(x)2\pi x dx$ where the Bessel function of the first kind, first order is

$$J_1(kx) = \frac{kx}{2} \left(1 - \frac{k^2 x^2}{2^2 1! 2!} + \frac{k^4 x^4}{2^4 2! 3!} - \frac{k^6 x^6}{2^6 3! 4!} + \dots \right) \quad (5.11)$$

This is similar to the differential procedure of

$$J'_0(kx) = \frac{dJ_0(kx)}{d(kx)} = -J_1(kx) \quad (5.12)$$

The terms of $J_0(kx)$ and $J_1(kx)$ can be divided into real and imaginary parts and are termed:

$$J_0(kx) = ber_0(mx) + jbei_0(mx) = M_0(mx)e^{i\theta_0(mx)} \quad (5.13)$$

$$J_1(kx) = ber_1(mx) + jbei_1(mx) = M_1(mx)e^{i\theta_1(mx)} \quad (5.14)$$

The current density at the axis is calculated as

$$s_0 = \frac{I}{2\pi a} \frac{k}{J_1(ka)} \quad (5.15)$$

where the total current of the conductor is

$$I = 2\pi s_0 \int_0^a J_0(kx)x dx = \frac{2\pi s_0}{k} [xJ_1(kx)]_0^a = \frac{2\pi s_0}{k} aJ_1(ka) \quad (5.16)$$

and

$$m^2 = \frac{\omega\mu_0}{\rho} = jk^2 \quad (5.17)$$

The above derivation was necessary to understand the process of skin effect entirely. This extensive derivation of the current density in conductor wires based on the effect of skin effect is visualized in the following figures. Figure 5.2 depicts the unequal current distribution inside of a conductor at various frequencies. For common frequencies of 50 Hz and 60 Hz the current distribution to the outside of the conductor is marginal in comparison to a higher frequency of 400 Hz as can be seen in Figure 5.3. Lower frequencies around 50 and 60 Hz range up to 1.07 increased current distribution on the outside, whereas 400 Hz amount to 1.28.

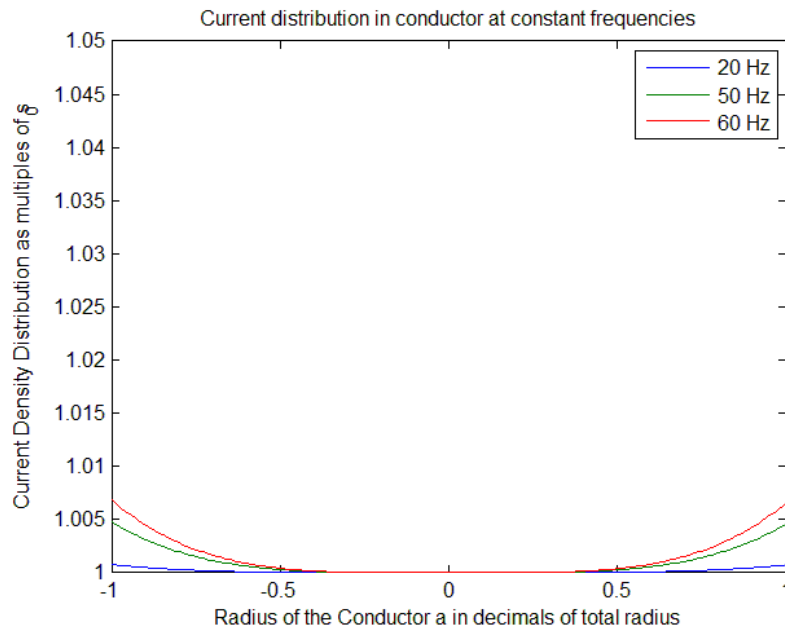


Figure 5. 2: Internal conductor current distribution for 20 Hz, 50 Hz, and 60 Hz

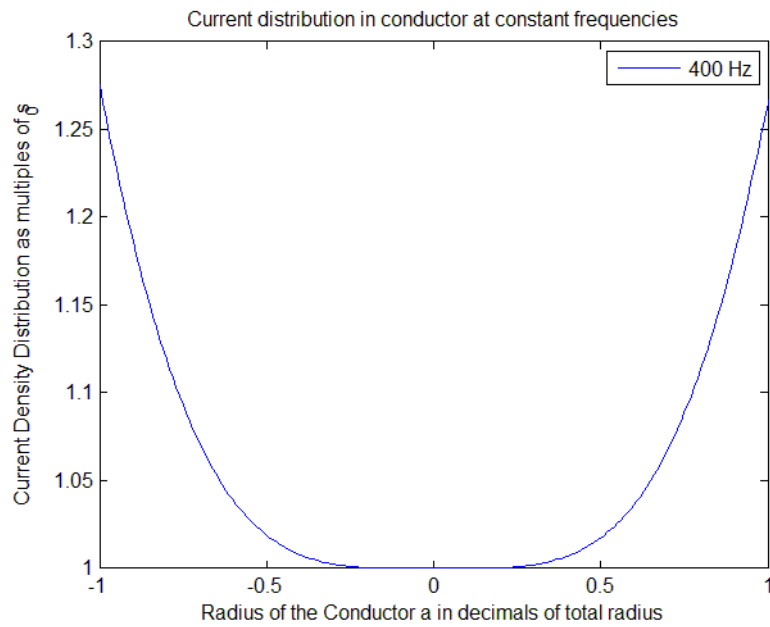


Figure 5. 3: Internal conductor current distribution for 400 Hz

A circulating current inside of a conductor adds to the losses. At higher frequencies tubular conductors not only save material, but also create smaller losses because the circulating current is decreased. The complex ohmic voltage drop at the conductor surface is

$$V_i = \frac{1}{2} I r_{d-c} ma \frac{M_0(ma)}{M_1(ma)} \angle(\theta_0(ma) - \theta_1(ma) + \frac{3\pi}{4}) \text{ volts/mile} \quad (5.18)$$

The corresponding impedance to the internal flux linkages and resistance of the conductor is

$$z_i = \frac{V_i}{I} = r_{d-c} \frac{ma}{2} \frac{M_0(ma)}{M_1(ma)} \angle(\theta_0(ma) - \theta_1(ma) + \frac{3\pi}{4}) \text{ ohms/mile} \quad (5.20)$$

where the imaginary component of z_i turns out to be

$$x_i = r_{d-c} \frac{ma}{2} \frac{M_0(ma)}{M_1(ma)} \sin \left[\theta_0(ma) - \theta_1(ma) + \frac{3\pi}{4} \right] \text{ ohms/mile} \quad (5.21)$$

And the real part being

$$r_{a-c} = r_{d-c} \frac{ma}{2} \frac{M_0(ma)}{M_1(ma)} \cos \left[\theta_0(ma) - \theta_1(ma) + \frac{3\pi}{4} \right] \text{ ohms/mile} \quad (5.22)$$

5.2 IMPEDANCE VARIATION THROUGH CHANGES IN FREQUENCY

The ratios of imaginary- and real- components taking the skin effect into consideration from 0 to 60 Hz are shown in Figure 5.4 and Figure 5.5. These figures depict the results for a 0.005 m thick conductor wire.

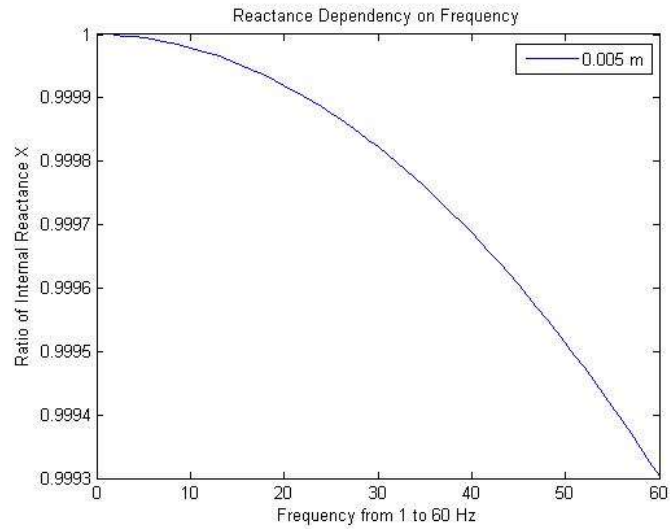


Figure 5. 4: Reactance Dependency on Frequency for a 5mm conductor

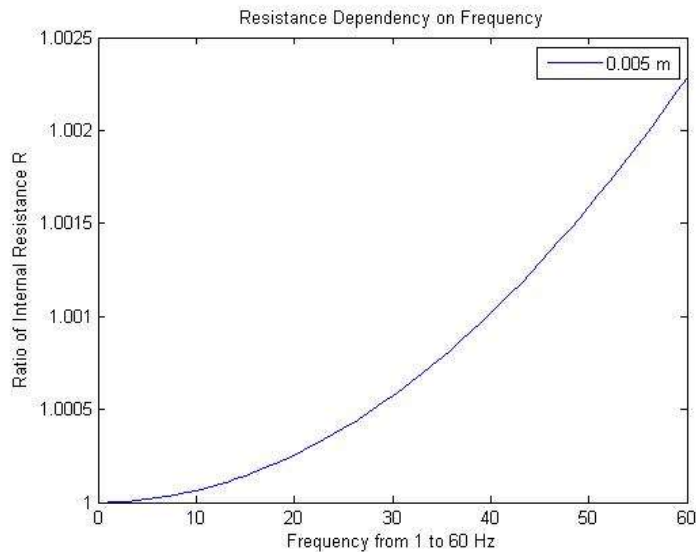


Figure 5. 5: Resistance Dependency on Frequency for a 5mm conductor

The ratio of internal reactance X decreases to 0.9993 with an increase in frequency up to 60 Hz, whereas the ratio of internal resistance R increases to 1.0023. This depicts the phenomenon, that with increasing frequency the reactance decreases and the resistance

increases. Figure 5.6 and Figure 5.7 depict the continuation of the previous graph but up to a higher frequency of 400 Hz.

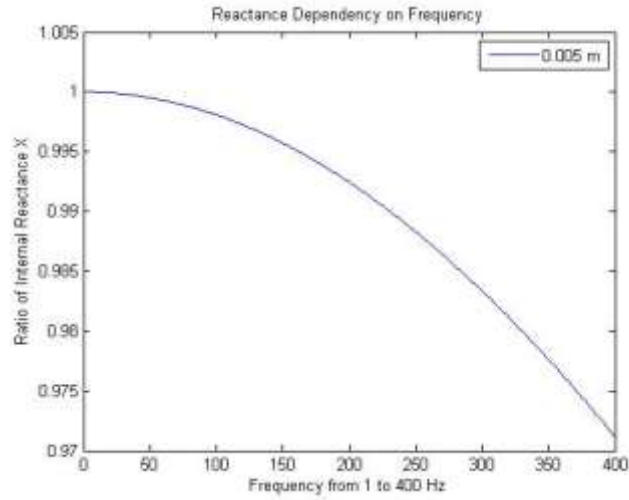


Figure 5. 6: Reactance Dependency on Frequency up to 400 Hz

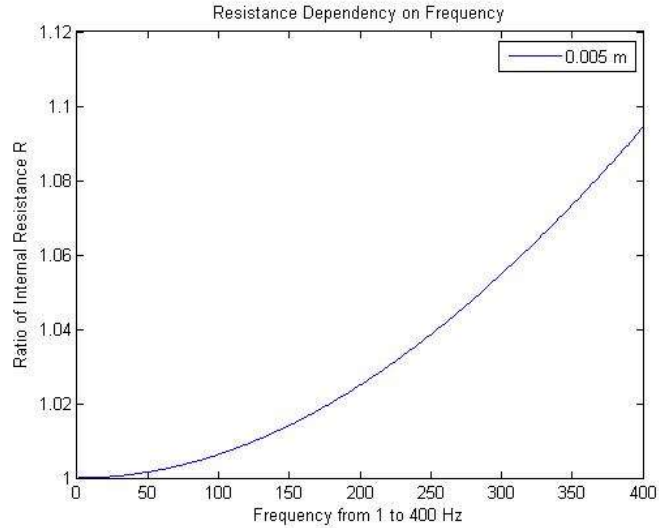


Figure 5. 7: Resistance Dependency on Frequency up to 400 Hz

These illustrations clarify how marginal the skin effect is in frequencies ranging up to 60 Hz. If impedance values are regarded for up to 400 Hz it becomes obvious that skin effect only plays a large role in higher frequency environments. The internal reactance X at a frequency of 400 Hz decreases to 0.972 and the internal resistance increases to a ratio of 1.095. The effect of different conductor thicknesses is visualized in Figure 5.8 and Figure 5.9.

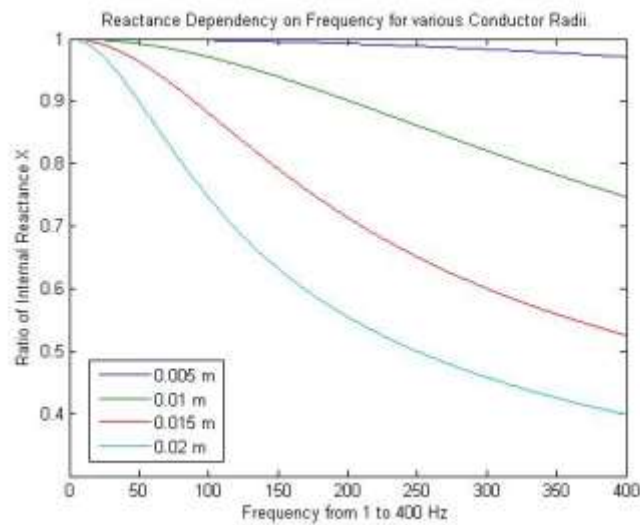


Figure 5. 8: Reactance Dependency for various Conductor Sizes

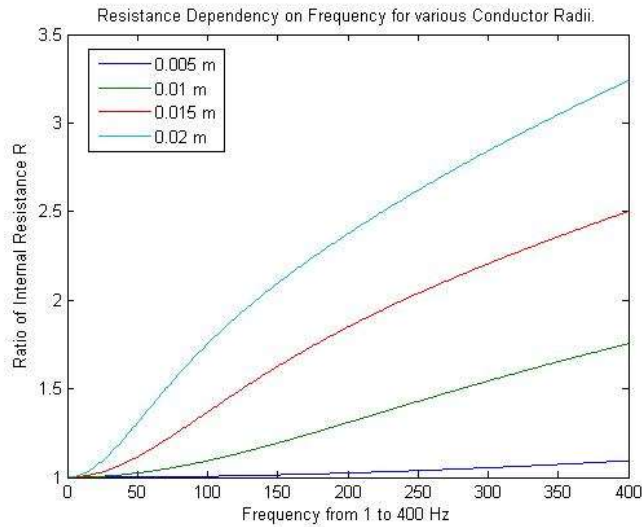


Figure 5. 9: Resistance Dependency for various Conductor Sizes

The bigger the radius of the conductor, the larger the skin effect on the ratio of internal reactance X and resistance R . For a theoretical conductor thickness of 0.02m which is equivalent to 0.787 inches the reactance decreases to a ratio of 0.85 at 60 Hz and to 0.4 at 400 Hz. The resistance ratio increases to 1.5 at 60 Hz and to 3.2 at 400 Hz. By analyzing the obtained results of skin effect it can be seen that in general, the conductors are hardly affected at frequencies up to 60 Hz. However, if the conductor radius is increased largely skin effect plays a bigger role, even in lower frequency environments. Hence, if conductors consist of thick wires skin effect might lead to significant inaccuracies in the calculation of internal line parameters. The 400 Hz illustrations are irrelevant in the analysis of transmission lines, but give good insight into the skin effect characteristics.

6. CONCLUSION

Based on the results obtained in the previous chapters multiple conclusions can be drawn. All PSCAD model simulations and results of the MATLAB evaluation of transmission line parameter calculations for grounding of shield wire and skin effect have been reviewed and evaluated. It can be concluded that both assumptions do not have a significant impact on the variation of line parameters. As previously mentioned in Chapter 5, only zero-sequence impedance is affected when tower footing is taken into consideration. Two-ended methods are not affected by the shield wire at all, whereas one-ended methods experience a small increase in error. The increase in error, however, is small and the assumption of a direct connection of the shield wire to ground is valid.

Skin effect ranging from 0 to 60 Hz does not change the internal reactance and resistance of the conductor drastically. Only at higher frequencies above 100 Hz does this effect significantly impact line parameter calculations and accuracy of algorithms. Hence, it is acceptable to assume the current distribution in a transmission line to be uniformly distributed.

6.1. SUMMARY OF DATA ANALYSIS

The PSCAD models and MATLAB simulations aimed to analyze the effect of line parameter assumptions and simplifications on the accurate representation of line parameters. Tower footing resistance only affects the zero-sequence line impedance. Since one-ended methods require the input of zero-sequence line impedance to estimate the location of single line-to-ground or double line-to-ground faults, the accuracy of these methods are affected by the presence of a tower footing resistance. The increase in error

is, however, small. The analysis also concludes that the size of the tower footing resistance, whether 5 or 100 Ω , has a marginal impact on fault location algorithms. Hence, an increase in the tower footing resistance only slightly changes the value of the zero-sequence line impedance. The number of towers between the monitoring location and the fault also does not have a significant impact on the accuracy of one-ended methods. In contrast, two-ended methods are robust to the presence of the tower footing resistance since they do not use zero-sequence line impedance in fault location computation. With a small increase in inaccuracy, it can be concluded that for performing line impedance calculations, shield wires can be assumed grounded directly to the earth, although in reality they are effectively grounded through tower footing resistances. The corresponding impact on one-ended fault locating algorithms is minor.

Based on the results obtained in Chapter 6, skin effect does not have any significant impact on line parameters when standard transmission line frequencies of 0 to 60 Hz are regarded. The change in reactance and resistance size is insignificantly small compared to larger frequencies. However, if the conductor radius is increased skin-effect increases and might have a considerable impact on reactance and resistance values. Hence, if conductors consist of thick wires skin effect might lead to significant inaccuracies in the calculation of internal line parameters. The procedure of stranded wiring in a single conductor was not analyzed in this thesis and might have an additional impact on the role of skin effect in thicker wires.

6.2. FUTURE WORK

Despite the fact that these assumptions only lead to minor inaccuracies in the parameter calculation, these approaches are essential for future implementations. With the shift to more dynamic and unstable electricity grids due to renewable energies and multiple energy sources at various locations, it is essential to use advanced and flexible computational procedures to simulate the electricity grid as accurately as possible. This means also calculating the line parameters of the transmission grid more dynamically. The above procedures should be integrated in a stand-alone module or integrated into existing technology and compared to the previously performed calculations. In particular, fault location algorithms would serve well to analyze the accuracy of these assumptions in real time.

Further, increasing amounts of harmonics in the electricity grid change the behavior and parameter values. These approaches should be analyzed in detail and included into the future work of dynamic line parameter calculation. Stranding and bundling were not taken into consideration for skin effect, but should be analyzed for future work. Only by implementing these algorithms in a real device and testing it in different environments further knowledge can be gained.

BIBLIOGRAPHY

- [1] "IEEE Guide for Determining Fault Location on AC Transmission and Distribution Lines," *IEEE Std C37.114-2004*, pp. 1-36, 2005.
- [2] J. D. Glover and M. S. Sarma, *Power System Analysis and Design*, Pacific Grove, CA: Wadsworth Group, 2002.
- [3] Westinghouse Electric and Manufacturing Co., *Electrical Transmission and Distribution Reference Book*, East Pittsburgh, PA: The Lakeside Press, 1944.
- [4] W. contributors, "Electrical resistivity and conductivity," Wikipedia, The Free Encyclopedia, 26 06 2014. [Online]. Available: http://en.wikipedia.org/wiki/Electrical_resistivity_and_conductivity. [Accessed 17 07 2014].
- [5] AVID CMS, "sipex.aq," SIPEX, [Online]. Available: <http://www.sipex.aq/access/page/index.html%3Fpage=92ba0e1a-c9dc-102a-8ea7-0019b9ea7c60.html>. [Accessed 28 6 2014].
- [6] CECEC Electric, "transmission-line.cn," Engineering and Designing for Transmission Lines, [Online]. Available: <http://www.transmission-line.cn/ACSR%20&%20AAC%20Conductors.htm>. [Accessed 27 6 2014].
- [7] Georgia State University, "Hyperphysics.phy," 2014. [Online]. Available: <http://hyperphysics.phy-astr.gsu.edu/hbase/electric/gaulaw.html>. [Accessed 29 6 2014].
- [8] openstax cnx, "open stax college," 6 6 2012. [Online]. Available: <http://cnx.org/content/m42317/latest/?collection=col11406/latest>. [Accessed 29 6 2014].
- [9] Wikipedia contributors, "Overhead power line," Wikipedia, The Free Encyclopedia, 13 7 2014. [Online]. Available: http://en.wikipedia.org/w/index.php?title=Overhead_power_line&oldid=616825351. [Accessed 17 7 2014].

- [10] J. Traphoner, S. Das and S. Santoso, "Impact of Grounded Shield Wire Assumption on Impedance-based Fault Location Algorithms," in *IEEE/PES General Meeting*, Washington D.C., 2014.
- [11] EPRI, "Distribution Fault Location: Field Data and Analysis 1012438," EPRI, PaloAlto, CA, 2006.
- [12] MCD Geosciences and Engineering, "sinkhole-expert.com," 2011. [Online]. Available: <http://sinkhole-expert.com/wp-content/uploads/photo-5a.jpg>. [Accessed 16 7 2014].
- [13] Google APIS, [Online]. Available: <http://patentimages.storage.googleapis.com/EP2194623A1/imgf0001.png>. [Accessed 29 7 2014].
- [14] A. Deri, A. Tevan and S. a. A. Castanheira, "The Complex Ground Return Plane: A Simplified Model for Homogeneous and Multi-Layer Earth Return," in *IEEE Transcation on Power Apparatus and Systems*, 1981.
- [15] W. H. Kersting, *Distribution System Modeling and Analysis*, 3rd ed., CRC Press, 2012.
- [16] Manitoba HVDC Research Center Inc., "Applications of PSCAD/EMTDC".
- [17] L. Eriksson, M. M. Saha and G. D. Rockefeller, "An Accurate Fault Locator With Compensation For Apparent Reactance In The Fault Resistance Resulting From Remote-End Infeed," *IEEE Transactions on Power Apparatus and Systems*, Vols. PAS-104, no. 2, pp. 423-436, Feb. 1985.
- [18] J. Zaborszky and J. W. Rittenhouse, *Electric Power Transmission*, Troy: The Rensselaer Bookstore, 1969.
- [19] Wikipedia, The Free Encyclopedia, "Skin Effect," [Online]. Available: http://en.wikipedia.org/wiki/Skin_effect. [Accessed 27 6 2014].
- [20] W. L. Weeks, *Transmission and Distribution of Electrical Energy*, New York: Harper & Row, 1981.